AD

USAAMRDL TECHNICAL REPORT 71-71

EFFECT OF DYNAMICALLY INDUCED RADIAL-DISPLACEMENT PERTURBATIONS ON THE MAXIMUM STRENGTH OF INITIALLY IMPERFECT, CIRCULAR CYLINDRICAL SHELLS UNDER CONSTANT-RATE END SHORTENING

By

Joseph Mullen, Jr.

J. Mayers

February 1972

EUSTIS DIRECTORATE

U. S. ARMY AIR MOBILITY RESEARCH AND DEVELOPMENT LABORATORY

FORT EUSTIS, VIRGINIA

CONTRACT DAAJ02-70-C-0075

DEPARTMENT OF AERONAUTICS AND ASTRONAUTICS

STANFORD UNIVERSITY

STANFORD, CALIFORNIA

Approved for public release; distribution unlimited.

74

DISCLAIMERS

The findings in this report are not to be construed as an official Department of the Army position unless so designated by other authorized documents.

When Government drawings, specifications, or other data are used for any purpose other than in connection with a definitely related Government procurement operation, the United States Government thereby incurs no responsibility nor any obligation whatsoever; and the fact that the Government may have formulated, furnished, or in any way supplied the said drawings, specifications, or other data is not to be regarded by implication or otherwise as in any manner licensing the holder or any other person or corporation, or conveying any rights or permission, to manufacture, use, or sell any patented invention that may in any way be related thereto.

Trade names cited in this report do not consitute an official endorsement or approval of the use of such commercial hardware or software.

DISPOSITION INSTRUCTIONS

Destroy this report when no longer needed. Do not return it to the originator.

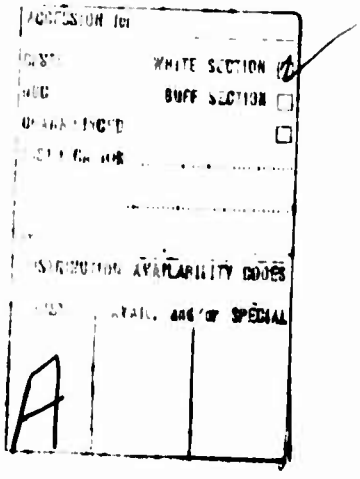

Unclassified

Security Classification

DOCUMENT CONTROL DATA - R & D

(Security classification of title, body of abstract and indexing annotation must be entered when the overall report is classified)

1. ORIGINATING ACTIVITY (Corporate author)	2a. REPORT SECURITY CLASSIFICATION
Stanford University Department of Aeronautics and Astronautics Stanford, California	Unclassified
	2b. GROUP N/A

3. REPORT TITLE

EFFECT OF DYNAMICALLY INDUCED RADIAL-DISPLACEMENT PERTURBATIONS ON THE MAXIMUM STRENGTH OF INITIALLY IMPERFECT, CIRCULAR CYLINDRICAL SHELLS UNDER CONSTANT-RATE END SHORTENING

4. DESCRIPTIVE NOTES (Type of report and inclusive dates)

Final Technical Report

5. AUTHOR(S) (First name, middle initial, last name)

Joseph Mullen, Jr.
Jean Mayers

6. REPORT DATE	7a. TOTAL NO. OF PAGES	7b. NO. OF REFS
February 1972	72	31

8a. CONTRACT OR GRANT NO.	9a. ORIGINATOR'S REPORT NUMBER(S)
DAAJ02-70-C-0075	USAAMRDL Technical Report 71-71
b. PROJECT NO.	
c. Task 1F061102A33F02	9b. OTHER REPORT NO(S) (Any other numbers that may be assigned this report)
d.	

10. DISTRIBUTION STATEMENT

Approved for public release; distribution unlimited.

11. SUPPLEMENTARY NOTES	12. SPONSORING MILITARY ACTIVITY
	Eustis Directorate U.S. Army Air Mobility R&D Laboratory Fort Eustis, Virginia

13. ABSTRACT

The effects of dynamic perturbations on the maximum strength of initially imperfect, axially compressed, circular cylindrical shells are studied using a modified Hamilton's principle based on a Reissner-type functional, von Kármán-Donnell shell kinematics, and a deformation theory of plasticity. The dynamic effects have been included by making use of the analogy of time-dependent imperfection growth to represent dynamic disturbance of the lateral motion of the shell wall. The results of the present analysis reflect families of load versus end-shortening curves for long circular cylinders. For each material, initial imperfection parameter, and radius-to-wall thickness ratio, there exist frequency-shortening rate ratios which provide unique load-end shortening paths in both the elastic and inelastic ranges. Significant maximum strength reductions are obtained for aluminum and stainless steel relative to the predictions of static elastic and inelastic theoretical analyses for shell radius-to-thickness ratios representative of closely stiffened and sandwich construction.

DD FORM 1 NOV 68 1473 REPLACES DD FORM 1473, 1 JAN 64, WHICH IS OBSOLETE FOR ARMY USE.

Unclassified

Security Classification

14. KEY WORDS	LINK A		LINK B		LINK C	
	ROLE	WT	ROLE	WT	ROLE	WT
Shells						
Maximum Strength						
Vibrations						
Failure Analysis						
Plasticity						

DEPARTMENT OF THE ARMY
U. S. ARMY AIR MOBILITY RESEARCH & DEVELOPMENT LABORATORY
EUSTIS DIRECTORATE
FORT EUSTIS, VIRGINIA 23604

This program was conducted under Contract DAAJ02-70-C-0075 with Stanford University, Stanford, California.

The data contained in this report are the results of research efforts to evaluate the effects of dynamic perturbations on the maximum strength of initially imperfect, axially compressed, circular cylindrical shells. The theory is based on a modified Hamilton's principle using a Reissner type functional, von Kármán-Donnell shell kinematics, and a deformation theory of plasticity. The results of the analysis reflect families of load versus end-shortening curves for long circular cylinders.

The report has been reviewed by this Directorate and is considered to be technically sound. It is published for the exchange of information and the stimulation of future research.

This program was conducted under the technical management of Mr. James P. Waller, Structures Division.

Task 1F061102A33F02
Contract DAAJ02-70-C-0075
USAAMRDL Technical Report 71-71
February 1972

EFFECT OF DYNAMICALLY INDUCED RADIAL-DISPLACEMENT PERTURBATIONS ON THE MAXIMUM STRENGTH OF INITIALLY IMPERFECT, CIRCULAR CYLINDRICAL SHELLS UNDER CONSTANT-RATE END SHORTENING

Final Report

By

Joseph Mullen, Jr.
J. Mayers

Prepared by

Department of Aeronautics and Astronautics
Stanford University
Stanford, California

for

EUSTIS DIRECTORATE
U. S. ARMY AIR MOBILITY RESEARCH AND DEVELOPMENT LABORATORY
FORT EUSTIS, VIRGINIA

ABSTRACT

The effects of dynamic perturbations on the maximum strength of initially imperfect, axially compressed, circular cylindrical shells are studied using a modified Hamilton's principle based on a Reissner-type functional, von Kármán-Donnell shell kinematics, and a deformation theory of plasticity. The dynamic effects have been included by making use of the analogy of time-dependent imperfection growth to represent dynamic disturbance of the lateral motion of the shell wall. The results of the present analysis reflect families of load versus end-shortening curves for long circular cylinders. For each material, initial imperfection parameter, and radius-to-wall thickness ratio, there exist frequency-shortening rate ratios which provide unique load-end shortening paths in both the elastic and inelastic ranges. Significant maximum strength reductions are obtained for aluminum and stainless steel relative to the predictions of static elastic and inelastic theoretical analyses for shell radius-to-thickness ratios representative of closely stiffened and sandwich construction.

FOREWORD

The work reported herein constitutes a portion of the effort being undertaken at Stanford University for the Eustis Directorate, U.S. Army Air Mobility Research and Development Laboratory under Contract DAAJ02-70-C-0075 (Task 1F061102A33F02). The present program is one of a series aimed at establishing accurate theoretical prediction capability for the static and dynamic behavior of aircraft structural components using both conventional and unconventional materials. Predecessor contracts supported investigations which led, in part, to the results presented in References 10, 13, 14, 15, 20, 38, and 31.

TABLE OF CONTENTS

LIST OF ILLUSTRATIONS

LIST OF SYMBOLS

A_{ij}	nondimensional direct stress coefficient
a_{ij}, b_{ij}, d_{ij}	nondimensional bending stress coefficients
E	Young's modulus, psi
E_S	secant modulus, psi
e	unit end shortening, in./in.
F'	stress energy density, psi
$\bar{H}''$	nondimensional form of modified Hamiltonian
h	distance separating middle surfaces of faces of two-element, isotropic cylinder, in.
K	nondimensional Ramberg-Osgood material constant
L	length of cylinder, in.
M_x, M_y	bending moments per unit length in x- and y-directions, respectively, lb
M_{xy}	twisting moment per unit length, lb
m	number of axial waves
N	nondimensional Ramberg-Osgood material constant
n	number of circumferential waves
R	radius of cylinder, in.
T''	kinetic energy, lb-in.
t	thickness of homogeneous, isotropic cylinder, in.

t_f	thickness of face sheet of two-element cylinder, in.
t_1, t_2	arbitrary time limits of integration, sec
U''	Reissner functional, lb-in.
$\overline{U}''$	nondimensional Reissner functional
V	volume, $in.^3$
u,v	middle-surface displacements in x- and y-directions, respectively, in.
w	middle-surface displacement in z-direction, in.
w_o	initial deviation of midsurface displacement in radial direction, in.
Δw_o	growth in initial displacement w_o due to dynamic disturbance, in.
x,y,z	cylinder coordinates, in.
γ_{xy}	total shear strain in the xy-plane, in./in.
γ'_{xy}	shear strain at middle surface, in./in.
γ''_{xy}	shear strain due to twisting, in./in.
ϵ	uniaxial strain, in./in.
ϵ_{eff}	effective strain, in./in.
ϵ'_x, ϵ'_y	strains due to extension in x- and y-directions, respectively, in./in.
$\epsilon''_x, \epsilon''_y$	strains due to bending in x- and y-directions, respectively, in./in.
η	nondimensional waveform parameter, $\eta = n^2 h/R = (n^2 t)/(\sqrt{3} R)$

κ_x, κ_y	changes in curvature of shell middle surface in x- and y-directions, respectively, 1/in.
κ_{xy}	change in twist of shell middle surface, 1/in.
λ_x, λ_y	buckle half-wavelengths in x- and y-directions, respectively, in.
μ	nondimensional buckle aspect ratio, $\mu = \lambda_y/\lambda_x$
ν	nondimensional Poisson's ratio for isotropic cylinder
ξ_{ij}	nondimensional displacement coefficient
ξ_{ij_o}	nondimensional imperfection amplitude coefficient
ρ	mass density of shell material, lb-sec^2/ft^4
σ	average compressive stress; uniaxial stress, psi
σ_{eff}	effective stress, psi
σ_x, σ_y	total stresses in x- and y-directions, respectively, psi
σ_x', σ_y'	average direct stresses in x- and y-directions, respectively, psi
σ_x'', σ_y''	bending stresses in x- and y-directions, respectively, psi
τ	time, sec
τ_{xy}	total shear stress in xy-plane, psi
τ_{xy}'	average shear stress in xy-plane, psi
τ_{xy}''	shear stress due to twisting, psi
ω	circular frequency, rad/sec

SUBSCRIPTS

b	denotes bottom face of two-element model
eff	effective
f	denotes face sheet
i,j	integers
o	denotes initial radial imperfection amplitudes
t	denotes top face of two-element model
x,y,z	denotes longitudinal, circumferential, and radial directions, respectively

OPERATOR SYMBOLS

$d(\ )$	ordinary differential
$\partial(\ )$	partial differential
$\delta(\ )$	variation
$(\ )_{,}$	denotes partial differention with respect to coordinate(s) following comma (e.g., $w_{,xy} = \partial^2 w/\partial x \partial y$)
$(\dot{})$	denotes ordinary differential with respect to time (e.g., $\dot{w} = dw/dt$)

INTRODUCTION

The theoretical and experimental developments pertaining to thin shells in recent years have essentially been channeled into three distinct areas: buckling and postbuckling, free vibration, and impulsive or forced excitation. In each case, attempts have been made to resolve the discrepancies between classical theory predictions and experimental results. In general, developments in each area have taken place independently of the others.

Much of the work directed toward initial buckling and postbuckling has been surveyed in three comprehensive papers by Hoff[1,2] and Stein.[3] The strongest emphasis by investigators has been directed toward asymmetric buckling of thin-walled, circular cylindrical shells in axial compression. The consensus of both authors has attributed the discrepancies between theory and experiment for compressed shells to the combined effects of initial imperfections, prebuckling deformations, and boundary conditions. The theoretical work of Donnell and Wan[4] and Koiter,[5] for example, coupled with the experimental findings of Horton and Durham,[6] Babcock and Sechler,[7] and Almroth, Holmes and Brush[8] has amply demonstrated the significance of the presence of initial imperfections in the buckling of axially compressed shell structures. Lesser significance is attributed to prebuckling deformations and boundary conditions from either quantitative or practical considerations. However, not to be overlooked is the effect of inelastic deformations; this phenomenon was apparently appreciated by Donnell[9] in 1934 but not given serious attention until the past decade, commencing with the theoretical work of Mayers and Rehfield[10] and the experimental program of Edwards.[11]

With the use of variational principles, nonlinear stress-strain relations, and von Kármán's large-deflection strain-displacement relations, Mayers *et al.*[12,13] were able to show for axially compressed flat rectangular plates that unique material dependent and width-to-thickness dependent load-end shortening curves existed when compression beyond the classical

buckling load and into the inelastic range occurred. More recently, Mayers and Wesenberg[14,15] have been able to obtain material-dependent and radius-to-thickness ratio-dependent load-shortening curves for axially compressed cylinders with the use of a modified-Reissner variational principle, von Kármán-Donnell strain-displacement relations, and nonlinear constitutive relationships. Unlike their plate counterparts, the families of initial-imperfection-dependent load-shortening curves never, in reality, reach classical buckling load predictions. In the presence of imperfection-sensitive loading paths into the inelastic range, significant reductions in maximum strength for both stiffened and unstiffened shells occur. Such reductions are shown to be obtained relative to any theory making use of a linearized stress-strain law. Significant reductions result even though the average compressive stress at buckling is well below the 0.2% offset yield stress of the material and as low as the proportional limit stress for some materials.

With regard to vibration of thin shells, much of the early development done within the context of linearized theory is contained in the work of Rayleigh,[16] Love,[17] and Flügge.[18] In 1955, Reissner[19] made the first significant contribution to the solution of the nonlinear problem by showing the axial and circumferential inertia to be negligible for predominantly radial motion. It is noteworthy to mention that his results simplified to those derivable from von Kármán-Donnell theory. Reissner, however, selected the asymmetric chessboard deflection pattern of linear theory for his shell nonlinear vibration studies. This choice has been invalidated by subsequent work on periodic, nonlinear free vibrations of thin shells. Finally, Mayers and Wrenn[20] have shown that nonlinear, free vibrations of shells are nonperiodic in nature based upon minimum energy considerations.

The direction of this study has been to combine the effects of static maximum strength and vibration in the more encompassing area of dynamic stability. A number of subclasses of the field of dynamic stability

are mentioned here. Each combines the effects of external loading and kinematic displacement of the structure to obtain a particular effect. Varying combinations, as noted by Hoff,[21] have been classified as parametric resonance, impulsive loading, circulatory loading, aeroelasticity, and--the one most pertinent to this study--buckling in the test machine. The phenomena of resonance and aeroelasticity have been well studied through the years. They are related to the excitation of one of the natural frequencies of the structure in question until such time as the amplitude range surpasses some admissible bound. Impulsive loadings, on the other hand, have traditionally been associated with the massive application of load for short durations beyond the maximum permissible. Circulatory loading is not considered here due to the presence of special highly directional loading requirements.

Dynamic buckling criteria in an elastic testing machine have been studied in several specialized cases. Hoff[22] has shown the existence of constant total energy contour lines about three equilibrium points for a compressed imperfect column. Similarly, by approaching the problem through consideration of the effects of loading velocity in a testing machine, Hoff[21] was able to detect stress reversal before maximum load in the case of columns.

In the present work, the maximum strength behavior of axially compressed circular cylindrical shells in the presence of dynamic perturbations has been studied using a modified Hamilton's principle incorporating time-dependent imperfection growth as a suitable analog. Also incorporated as part of the variational principle is a modified form of Reissner's functional based upon the von Kármán-Donnell strain displacement relations. The allowance for the presence of the modified-Reissner functional facilitates the incorporation of inelastic effects by selection of the state of stress independently of the displacements (or state of strain). This procedure has been well established[13] and used with confidence for shells in References 14 and 15. On this basis, inelastic maximum strength, radius-to-thickness dependent load-shortening curves have been obtained.

The effects of the presence of dynamic perturbations are then studied not only in terms of the mechanism of buckling but also in terms of both shell radius-to-thickness ratio and material property dependency.

GENERAL THEORY

STATEMENT OF PROBLEM AND BASIC ASSUMPTIONS

The problem considered is that of the effect of dynamic perturbations in the maximum strength analysis of initially imperfect, axially compressed circular cylindrical shells. The end-shortening rather than the end-loading of the shell is prescribed; this corresponds to loading of the shell in a rigid testing machine. The approach to the solution has been to consider the physical interaction of free vibration in the deflected shape of the cylinder wall as a means of initiating growth in the initial imperfection shape. The differential equations of motion are reduced to their static equivalents and an additional, approximate sinusoidally vibrating deflection function is included to account for the effect of inertia.

The solution for the differential equations of motion for axially compressed, vibrating shells is obtained from a modified Hamilton's variational principle. Reissner's functional is substituted for the strain energy in order to provide arbitrariness in the selection of strain and stress states and to include the effects of nonlinear-elastic material behavior. In the statically equivalent system, no unloading in the nonlinear-elastic range is assumed to occur. In the assumed dynamic deflection function, only the first quarter-sine wave is considered. Since maximum strength is the criterion for comparison, the first maximum amplitude is all that need be included. As a result, the inelastic and nonlinear-elastic ranges can be considered as interchangeable. From the reduction of the differential equations of motion to their static equivalents, the results of Mayers and Wesenberg[14] are reproduced.

The basic two-element description of the shell cross section (Figure 1) previously used in plate and shell analyses (see References 12, 13, 14, 15) is adopted for the dynamic maximum strength analysis. This description in its simplest form is composed of two thin face sheets separated

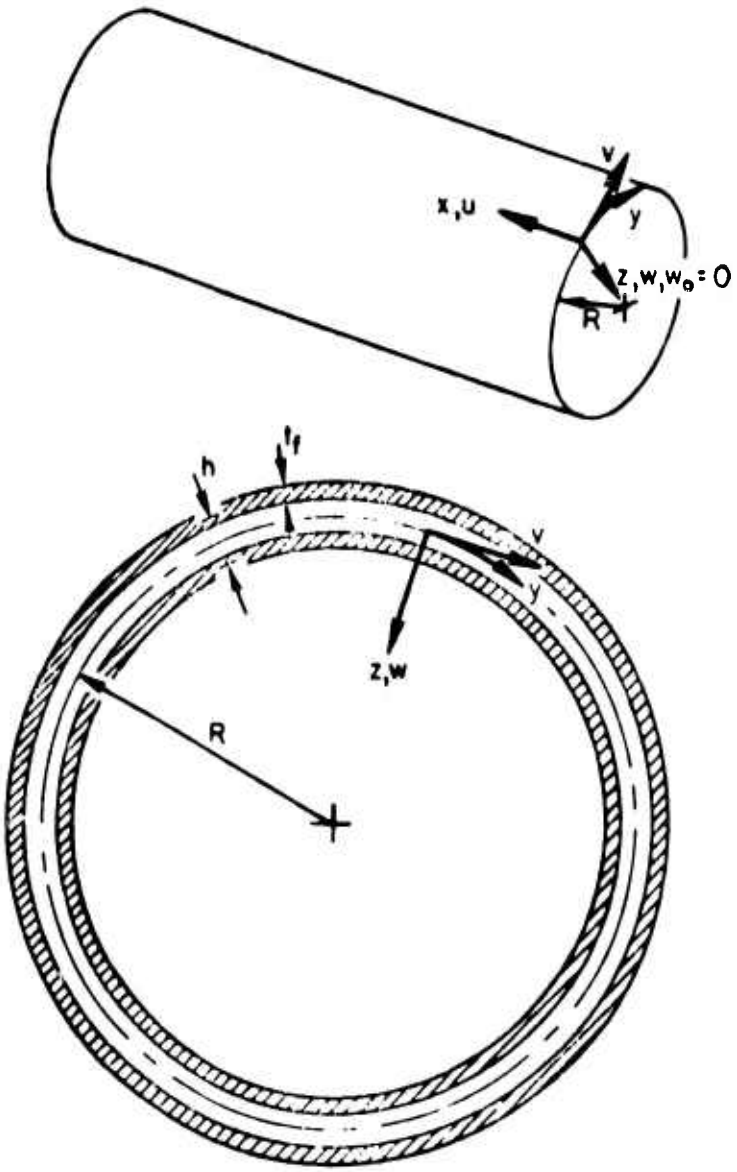

Figure 1. Circular Cylindrical Shell With Two-Element Cross Section.

by a non-stress-carrying core. The stress distribution is considered to be constant across the thickness of any face sheet, and the complexities of integrating a nonlinear stress distribution through the shell thickness are conveniently avoided. The core is considered to be infinitely rigid in shear and normal compression; the shell behavior is based on von Kármán-Donnell large displacement theory. In general, material compressibility effects are considered to be negligible and Poisson's ratio is taken as $\nu = 0.5$ for computations. The constitutive equations used to describe the nonlinear material properties make use of the Ramberg-Osgood[23] power law stress-strain curve approximation for aircraft structural metals.

The von Kármán-Donnell strain-displacement equations have been adopted for the two-element, initially imperfect shell. For radial deflection-thickness ratio magnitudes of the order of one in the prebuckling or initial buckling state, and in view of the conclusions of Mayers and Rehfield,[10] the von Kármán-Donnell strain-displacement relations are justifiable.

BASIC EQUATIONS

The von Kármán-Donnell strain-displacement relations for the isotropic two-element cylinder, modified to include the effects of initial radial imperfections, as shown in Reference 14, are

$$\begin{aligned}
\epsilon'_x &= u_{,x} + \frac{1}{2} w_{,x}^2 + w_{,x} w_{o,x} \\
\epsilon'_y &= v_{,y} + \frac{1}{2} w_{,y}^2 + w_{,y} w_{o,y} - \frac{w}{R} \\
\gamma'_{xy} &= u_{,y} + v_{,x} + w_{,x} w_{,y} + w_{o,x} w_{,y} + w_{,x} w_{o,y}
\end{aligned} \tag{1}$$

The curvature-displacement relations are given by

$$\kappa_x = - w_{,xx}$$

and

$$\kappa_y = -w_{,yy}$$

$$\kappa_{xy} = -w_{,xy} \tag{2}$$

The total strains for the top and bottom faces of the two-element isotropic cylinder become, respectively,

$$\epsilon_{x_{t,b}} = \epsilon'_x \pm z\kappa_x$$

$$\epsilon_{y_{t,b}} = \epsilon'_y \pm z\kappa_y$$

$$\gamma_{xy_{t,b}} = \gamma'_{xy} \pm 2z\kappa_{xy} \tag{3}$$

REISSNER FUNCTIONAL

The Reissner variational principle requires the vanishing of the first variation of both the free states of stress and strain for equilibrium and stress-displacement compatibility. The requirements for admissible variations are the enforcement of the boundary conditions on the prescribed surface displacements and their continuity throughout the body. For plates and shells, the Reissner functional is

$$U'' = \iiint_V \left\{ \sigma_x \epsilon_x + \sigma_y \epsilon_y + \tau_{xy} \gamma_{xy} - F' \right\} dV \tag{4}$$

where F' is the stress-energy density. F' is the energy function which for incremental changes in stress relates the strains at every point by the expressions

$$\epsilon_x = \frac{\partial F'}{\partial \sigma_x} \quad , \quad \epsilon_y = \frac{\partial F'}{\partial \sigma_y} \quad , \quad \gamma_{xy} = \frac{\partial F'}{\partial \tau_{xy}} \tag{5}$$

KINETIC ENERGY

The two-dimensional kinetic energy expression is the sum of the incremental longitudinal, circumferential, and lateral motions of the cylinder. For the analysis of thin shells, rotational inertia effects are neglected. The kinetic energy then becomes the sum of the kinetic energies associated with the axial, circumferential, and radial velocities of the cylinder, or

$$T'' = \iiint_V \frac{1}{2} \rho \left[\dot{u}^2 + \dot{v}^2 + \dot{w}^2 \right] dxdydz \tag{6}$$

Integration over the depth of the two-element cylinder of face thicknesses t_f gives

$$T'' = \frac{1}{2} \rho (2t_f) \int_0^L \int_0^{2\pi R} \left[\dot{u}^2 + \dot{v}^2 + \dot{w}^2 \right] dxdy \tag{7}$$

for constant ρ .

STRESS-ENERGY DENSITY

For linear-elastic problems, F' becomes the complementary energy density and Reissner's functional can be reduced to the strain energy with the enforcement of Hooke's law. As developed in Reference 12 for nonlinear elastic materials, the stress energy density F' is given by

$$F' = \int_0^{\sigma_{eff}} \epsilon_{eff} d\sigma_{eff} \tag{8}$$

where from the secant-modulus deformation theory of plasticity the "effective" stress is written as

$$\sigma_{eff}^2 = \sigma_x^2 + \sigma_y^2 - 2\nu\sigma_x\sigma_y + 2(1+\nu)\,\tau_{xy}^2 \tag{9}$$

for an isotropic material and ν is understood to equal $\frac{1}{2}$.

In turn, "effective" stress is related to "effective" strain by the secant-modulus of the uniaxial stress-strain curve of the material as

$$\sigma_{eff} = E_S \epsilon_{eff} \tag{10}$$

In the present analysis developments, the uniaxial stress-strain curves in tension and compression are taken as identical.

Upon substitution for the stress energy density, Reissner's functional may then be written as

$$U'' = \iiint_V \left\{ \sigma_x \epsilon_x + \sigma_y \epsilon_y + \tau_{xy} \gamma_{xy} - \int_0^{\sigma_{eff}} \epsilon_{eff} d\sigma_{eff} \right\} dV \tag{11}$$

For the purposes of this analysis the nonlinear relationship between stress and strain is that developed by Ramberg and Osgood.[23] This three-parameter representation of the uniaxial stress-strain curve is written as a power function in the form

$$\epsilon_{eff} = \left(\frac{\sigma_{eff}}{E} \right) + K \left(\frac{\sigma_{eff}}{E} \right)^N \tag{12}$$

where E , K , and N are the material constants for a given material. For the present analysis, this form is used without regard to the effects of unloading. Previous work involving inelastic effects in the bending, buckling, and postbuckling of plates and shells indicates that only localized unloading of small magnitude takes place at buckling.

The functional U'' integrates to

$$U'' = \iiint_V \left\{ \sigma_x \epsilon_x + \sigma_y \epsilon_y + \tau_{xy} \gamma_{xy} - \left[\frac{\sigma_{eff}^2}{2E} + \frac{KE}{N+1} \left(\frac{\sigma_{eff}}{E} \right)^{N+1} \right] \right\} dV \tag{13}$$

Consistent with the two-element description developed in Appendix I, integration of Reissner's functional over the depth, h , yields

in terms of the midsurface direct and bending stress, the strain components, and the "effective" stress

$$
\begin{aligned}
U'' = 2t_f \int_0^L \int_0^{2\pi R} \Big\{ & \sigma'_x \epsilon'_x + \sigma'_y \epsilon'_y + \tau'_{xy} \gamma'_{xy} \\
& + \sigma''_x \epsilon''_x + \sigma''_y \epsilon''_y + \tau''_{xy} \gamma''_{xy} \\
& - \frac{1}{2} \left[\sigma'^2_x + \sigma'^2_y - 2\nu\, \sigma'_x \sigma'_y + 2(1+\nu)\, \tau'^2_{xy} \right. \\
& \left. + \sigma''^2_x + \sigma''^2_y - 2\nu\, \sigma''_x \sigma''_y + 2(1+\nu)\, \tau''^2_{xy} \right] \\
& - \frac{1}{2} \frac{KE}{N+1} \left[\left(\frac{\sigma_{eff}}{E} \right)^{N+1}_t + \left(\frac{\sigma_{eff}}{E} \right)^{N+1}_b \right] \Big\} \, dxdy
\end{aligned}
\tag{14}
$$

where the "t" and "b" subscripts refer to the top and bottom faces of the two-element cross section, respectively. Finally, with the addition of the von Kármán-Donnell strain-displacement relations, the Reissner functional becomes

$$
\begin{aligned}
\frac{U''}{2t_f E} = \int_0^L \int_0^{2\pi R} \Big\{ & \frac{\sigma'_x}{E} \left[u_{,x} + \frac{1}{2} w^2_{,x} + w_{o,x} w_{,x} \right] \\
& + \frac{\sigma'_y}{E} \left[v_{,y} + \frac{1}{2} w^2_{,y} + w_{o,y} w_{,y} - \frac{w}{R} \right] \\
& + \frac{\tau'_{xy}}{E} \left[u_{,y} + v_{,x} + w_{,x} w_{,y} + w_{o,x} w_{,y} + w_{o,y} w_{,x} \right] \\
& + \frac{\sigma''_x}{E} \left[\frac{h}{2} w_{,xx} \right] + \frac{\sigma''_y}{E} \left[\frac{h}{2} w_{,yy} \right] + \frac{\tau''_{xy}}{E} \left[h w_{,xy} \right]
\end{aligned}
$$

$$- \frac{1}{2}\left[\left(\frac{\sigma'_x}{E}\right)^2 + \left(\frac{\sigma'_y}{E}\right)^2 - 2\nu\left(\frac{\sigma'_x}{E}\right)\left(\frac{\sigma'_y}{E}\right) + 2(1+\nu)\left(\frac{\tau'_{xy}}{E}\right)^2\right.$$

$$\left. + \left(\frac{\sigma''_x}{E}\right)^2 + \left(\frac{\sigma''_y}{E}\right)^2 - 2\nu\left(\frac{\sigma''_x}{E}\right)\left(\frac{\sigma''_y}{E}\right) + 2(1+\nu)\left(\frac{\tau''_{xy}}{E}\right)^2\right]$$

$$\left. - \frac{K}{2(N+1)}\left[\left(\frac{\sigma_{eff}}{E}\right)^{N+1}_t + \left(\frac{\sigma_{eff}}{E}\right)^{N+1}_b\right]\right\} dxdy \qquad (15)$$

The kinetic energy is combined with the Reissner functional in the form of a modified Lagrangian. When integrated over a given time period, this yields the Hamiltonian in the form

$$\int_{t_1}^{t_2}\left(\frac{U''-T''}{2t_f E}\right)dt = \int_{t_1}^{t_2}\int_0^L\int_0^{2\pi R}\left\{\frac{\sigma'_x}{E}\left[u_{,x} + \frac{1}{2}w^2_{,x} + w_{o,x}w_{,x}\right]\right.$$

$$+ \frac{\sigma'_y}{E}\left[v_{,y} + \frac{1}{2}w^2_{,y} + w_{o,y}w_{,y} - \frac{w}{R}\right]$$

$$+ \frac{\tau'_{xy}}{E}\left[u_{,y} + v_{,x} + w_{,x}w_{,y} + w_{o,x}w_{,y} + w_{,x}w_{o,y}\right]$$

$$+ \frac{\sigma''_x}{E}\left[\frac{h}{2}w_{,xx}\right] + \frac{\sigma''_y}{E}\left[\frac{h}{2}w_{,yy}\right] + \frac{\tau''_{xy}}{E}\left[hw_{,xy}\right]$$

$$- \frac{1}{2}\left[\left(\frac{\sigma'_x}{E}\right)^2 + \left(\frac{\sigma'_y}{E}\right)^2 - 2\nu\left(\frac{\sigma'_x}{E}\right)\left(\frac{\sigma'_y}{E}\right) + 2(1+\nu)\left(\frac{\tau'_{xy}}{E}\right)^2\right.$$

$$\left. + \left(\frac{\sigma''_x}{E}\right)^2 + \left(\frac{\sigma''_y}{E}\right)^2 - 2\nu\left(\frac{\sigma''_x}{E}\right)\left(\frac{\sigma''_y}{E}\right) + 2(1+\nu)\left(\frac{\tau''_{xy}}{E}\right)^2\right]$$

$$- \frac{1}{2} \frac{K}{N+1} \left[\left(\frac{\sigma_{eff}}{E} \right)_t^{N+1} + \left(\frac{\sigma_{eff}}{E} \right)_b^{N+1} \right]$$

$$- \frac{1}{2} \frac{\rho}{E} \left[\dot{u}^2 + \dot{v}^2 + \dot{w}^2 \right] \Bigg\} dxdydt \qquad (16)$$

VARIATIONAL PRINCIPLE

The application of the modified-Hamilton's principle requires the vanishing of the first variation simultaneously with respect to the admissible degrees of freedom that characterize the states of stress and strain; this condition is indicated by the symbolic form

$$\delta_{u,v,w,\sigma_x,\sigma_y,\tau_{xy}} \int_{t_1}^{t_2} (U'' - T'') \, dt = 0 \qquad (17)$$

The prescribed, constant-rate end shortening $e(t)$ is included in $u(t)$; thus, a potential of applied loads term does not appear in the variational principle.

The application of this principle allows the independent variation of the states of stress and strain. The enforcement of the above condition results in the Euler equations of motion, the stress-displacement relations, and both the initial and boundary conditions. The system of Euler equations for the circular cylindrical shell which behaves according to the von Kármán-Donnell strain-displacement relations is developed in Appendix I for the two-element model representation of the actual cylinder.

METHOD OF SOLUTION

Investigators in the past have approached the maximum strength and nonlinear vibration problems as two distinct phenomena. In References 1-3, the major contributors to the linear-elastic buckling and post-buckling of shells to 1967 are listed. More recently, Mayers and Wesenberg[14,15] have extended theory and analysis to include inelastic effects. For nonlinear, free vibrations of shells, the literature is relatively sparse. Noteworthy contributions, all since 1955, are those of Reissner,[19] Evenson and Fulton,[24] and Mayers and Wrenn.[20]

The present analysis has taken the perspective of treating vibration as a time-dependent perturbation of initial imperfection in a shell which decreases the maximum strength. Thus, the analysis can proceed much like that of Mayers and Wesenberg[14] in its development of a solution. A prescribed constant-rate displacement of the shell edges permits an assumed time-dependent imperfection growth (perturbation) amplitude to be related to the end shortening.

DISPLACEMENT FORMULATIONS

The primary consideration in the choice of a displacement function is the prebuckling deformation pattern. The approach followed is to take the free stresses and radial deflection pattern in the same form as those formulated by Kempner.[25] Thus, the present analysis can be reduced to that of Kempner's in the perfect cylinder, linear-elastic, static case. Then, rather than specifying the stresses and strains as given functions of time, the unknown coefficients are allowed to vary freely and the differential equations of motion in terms of the initial and buckling patterns are obtained.

The radial displacement buckle pattern as specified by Kempner[25] is

$$w(t) = h\left[\xi_{00}(t) + \xi_{11}(t)\cos\frac{\pi x}{\lambda_x}\cos\frac{\pi y}{\lambda_y} + \xi_{20}(t)\cos\frac{2\pi x}{\lambda_x} + \xi_{02}(t)\cos\frac{2\pi y}{\lambda_y}\right] \tag{18}$$

where the wavelengths are $\lambda_x = L/m$ and $\lambda_y = \pi R/n$, respectively. For prescribed end shortening, the choice of the corresponding midsurface displacements is

$$u = -ex$$
$$v = 0 \tag{19}$$

where $e = \dot{e}t$ is the unit end shortening and $\dot{e}$ is the constant unit end-shortening rate.

The assumption of midsurface-displacement functions reflecting no free parameters has been justified in References 10, 13, 14, and 15. This simplification takes cognizance of the fact that either nonexistent or only very weak coupling can be assumed to occur between the midsurface stresses and strains in the Reissner formulation of the shell bending and buckling problem with only lateral equilibrium being satisfied by application of the variational principle. An analogous simplification in the shell vibration problem is attributed to Reissner;[19] as long as the inertia effects are primarily the results of transverse vibration, longitudinal inertia effects can be neglected. As shown in Appendix I, the simplification in the u- and v-displacement choices permits satisfaction of the middle-surface equilibrium equations independently of the magnitudes of the free stress coefficients.

STRESS FORMULATIONS

The membrane stresses are

$$\frac{\sigma_x'(t)}{E} = -\left[\frac{\sigma(t)}{E} + A_{11}(t)\cos\frac{\pi x}{\lambda_x}\cos\frac{\pi y}{\lambda_y} + 4A_{22}(t)\cos\frac{2\pi x}{\lambda_x}\cos\frac{2\pi y}{\lambda_y} + 9A_{13}(t)\cos\frac{\pi x}{\lambda_x}\cos\frac{3\pi y}{\lambda_y} + A_{31}(t)\cos\frac{3\pi x}{\lambda_x}\cos\frac{\pi y}{\lambda_y} + 4A_{02}(t)\cos\frac{2\pi y}{\lambda_y}\right]$$

and

$$\frac{\tau'_{xy}(t)}{E} = -\mu\left[A_{11}(t)\sin\frac{\pi x}{\lambda_x}\sin\frac{\pi y}{\lambda_y} + 4A_{22}(t)\sin\frac{2\pi x}{\lambda_x}\sin\frac{2\pi y}{\lambda_y} + 3A_{13}(t)\sin\frac{\pi x}{\lambda_x}\sin\frac{3\pi y}{\lambda_y} + 3A_{31}(t)\sin\frac{3\pi x}{\lambda_x}\sin\frac{\pi y}{\lambda_x}\right]$$

$$\frac{\sigma'_{y}(t)}{E} = -\mu^2\left[A_{11}(t)\cos\frac{\pi x}{\lambda_x}\cos\frac{\pi y}{\lambda_y} + 4A_{22}(t)\cos\frac{2\pi x}{\lambda_x} + A_{13}(t)\cos\frac{\pi x}{\lambda_x}\cos\frac{3\pi y}{\lambda_y} + 9A_{31}(t)\cos\frac{3\pi x}{\lambda_y}\cos\frac{\pi y}{\lambda_y} + 4A_{20}(t)\cos\frac{2\pi x}{\lambda_x}\right] \tag{20}$$

As shown in Appendix I, this set of stresses identically satisfies the middle-surface equilibrium equations for the x- and y-directions.

The bending stresses are chosen in the form of the curvatures, but with free coefficients to accommodate the general case of a nonlinear relationship between stress and strain. Thus,

$$\frac{\sigma''_{x}(t)}{E} = a_{11}(t)\cos\frac{\pi x}{\lambda_x}\cos\frac{\pi y}{\lambda_y} + a_{20}(t)\cos\frac{2\pi x}{\lambda_x} + a_{02}(t)\cos\frac{2\pi y}{\lambda_y}$$

$$\frac{\sigma''_{y}(t)}{E} = b_{11}(t)\cos\frac{\pi x}{\lambda_x}\cos\frac{\pi y}{\lambda_y} + b_{20}(t)\cos\frac{2\pi x}{\lambda_x} + b_{02}(t)\cos\frac{2\pi y}{\lambda_y}$$

$$\frac{\tau''_{xy}(t)}{E} = d_{11}(t)\sin\frac{\pi x}{\lambda_x}\sin\frac{\pi y}{\lambda_y} \tag{21}$$

INITIAL IMPERFECTION PATTERN

In the experimental work of Tennyson and Welles,[26] the first approximation to the radial deflection pattern at the onset of buckling was found to be composed of the asymmetric chessboard pattern plus an axisymmetric contribution corresponding to the second harmonic. Similarly, and with more significance to the present work, Mayers and Wrenn,[20] in their analysis of the nonlinear free vibrations of thin shells, determined that for radial deflections of the order of the shell thickness, the minimum energy solution corresponds to the chessboard pattern modified by a symmetric contribution corresponding to the second harmonic.

The choice of the imperfection pattern herein includes two components: the initial buckling shape ascribed to Tennyson and Welles[26] and used by Mayers and Wesenberg[14] in their maximum strength analysis, and an imperfection-growth component with the same modal shape but with time-varying amplitude. It is this prescribed growth component that provides the analogy to the presence of inertia in the equations of motion. The form of the initial imperfection is

$$w_o(t) = h\left[\left(\xi_{11_o} + \xi_{11_o} \sin \omega t\right) \cos \frac{\pi x}{\lambda_x} \cos \frac{\pi y}{\lambda_y} + \left(\xi_{20_o} + \xi_{20_o} \sin \omega t\right) \cos \frac{2\pi x}{\lambda_x}\right] \tag{22}$$

where, as a first approximation to dynamic perturbation on static maximum strength, simple harmonic motion is assumed to represent the imperfection growth pattern. Though nonlinear vibration of circular shells has been shown to be nonperiodic,[20] the primary interest here is in carrying the analysis through the first quarter-period of an imperfection-growth oscillation. At this time, the perturbation has reached its first maximum amplitude.

ELASTIC LOAD-SHORTENING RELATIONSHIP

With the displacement, stress, and imperfection functions given by Equations (18), (19), (20), (21), and (22), all of the quantities appearing in the functional, Equation (16), are defined and the variational principle indicated by Equation (17) can be applied. The integrated functional is given in Appendix II for the general case. With time-dependence neglected (static problem) and $K = 0$ (linear-elastic material), the Reissner functional reduces to that developed originally in Reference 14 and reproduced in Appendix III. For the present static problem, with $K = 0$, the vanishing of the first variation of Equation (16) with respect to ξ_{ij}, A_{ij}, a_{ij}, b_{ij}, d_{11}, and σ/E leads, after simplification, to just four equations in the four unknowns, ξ_{11}, ξ_{20}, ξ_{02}, and σ/E. Their solution for given imperfection growths and end-shortenings permits the construction of the linear-elastic material load-shortening curves shown in Figure 2.

INELASTIC LOAD-SHORTENING RELATIONSHIP

The equivalent inelastic static problem is obtained for nonvanishing K (nonlinear elastic material) in Equation (16). The inelastic load-shortening curves for the circular cylindrical shell are derived from the extrema of the following functional:

$$\frac{U''}{VE} = \left(\frac{U''}{VE}\right)_{elastic} - \frac{1}{2}\,\frac{K}{(N+1)} \int_0^1 \int_0^1 \left[\left(\frac{\sigma_{eff}}{E}\right)_t^{N+1} + \left(\frac{\sigma_{eff}}{E}\right)_b^{N+1}\right] \cdot$$

$$\cdot\, d\left(\frac{x}{L}\right)\, d\left(\frac{y}{2\pi R}\right) \qquad (23)$$

The vanishing of the first variation with respect to each of the 17 free parameters ξ_{ij}, A_{ij}, a_{ij}, b_{ij}, d_{11}, and σ/E is enforced to again obtain a system of imperfection-dependent load-shortening relationships. The presence of higher-order terms associated with

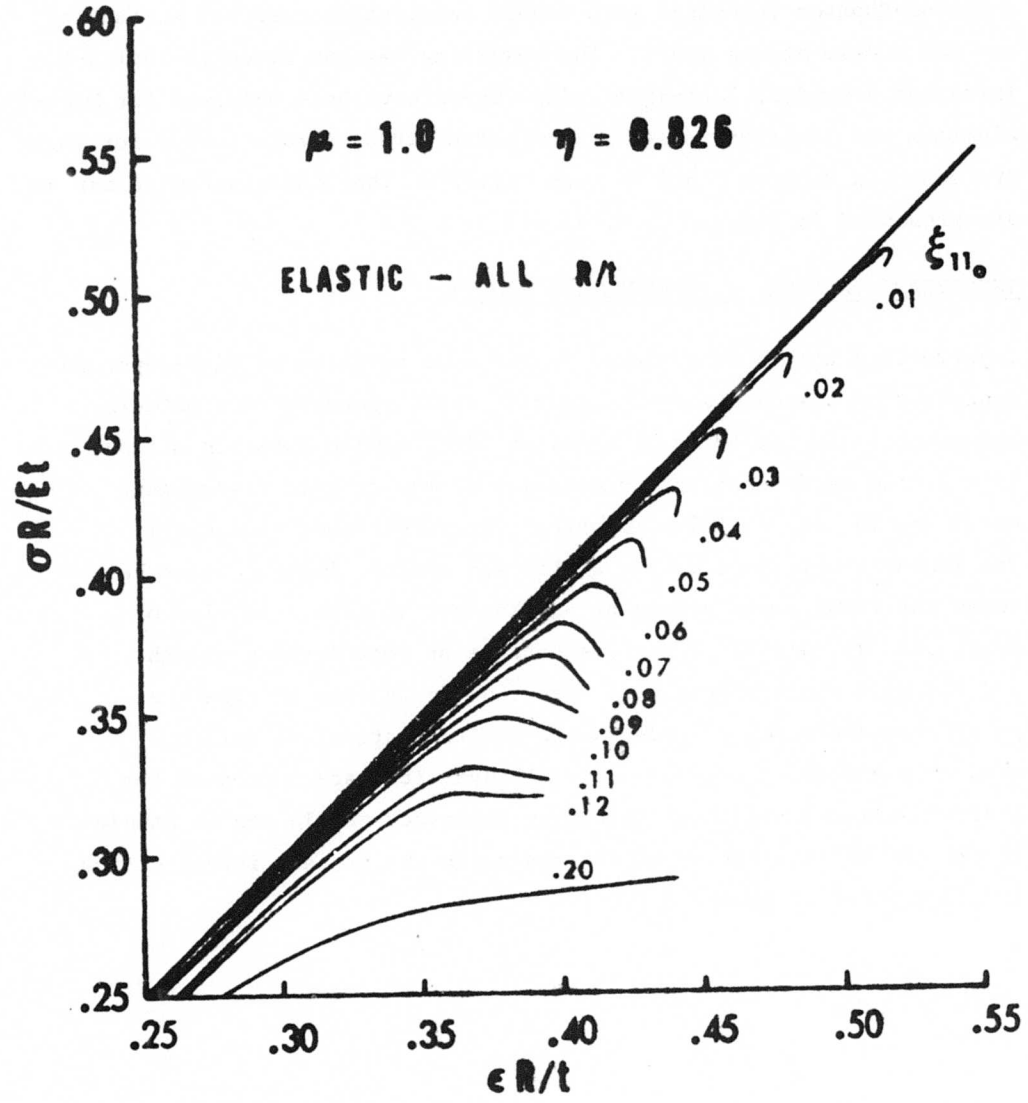

Figure 2. Family of Linear-Elastic, Imperfection-Sensitive, Load-Shortening Curves for a Two-Element Isotropic Cylinder.

nonzero values of K precludes any rational possibility of obtaining explicit relationships coupling any of the 17 free parameters. The solution for the extrema has been adopted for numerical solution using a Newton-Raphson technique with double integration over the surface of any one buckle of the shell. The resulting maximum-strength radius-to-thickness dependent load-shortening curves have been obtained for 2024-T3 aluminum and stainless steel ($\frac{1}{2}$ hard), the stress-strain curves for which are shown in Figures 3 and 4, respectively. The load-shortening curves are presented in Figures 5, 6, 7, 8.

THE DYNAMIC ANALOGY — IMPERFECTION GROWTH

Imperfection growth is achieved by the superposition of time-dependent imperfection components on the initial static imperfection pattern components. As indicated by Equation (22), simple harmonic motion is selected as describing the behavior of the dynamic disturbance occurring in the initially imperfect, uniformly shortened shell. The linear combination of the static and dynamic imperfections becomes the total imperfection at any instant in time. In view of Equations (19) and (22), the disturbance or imperfection growth and the unit end shortening e are coupled in time to create a phenomenon analogous to end-loading-excited lateral vibration. With this analog, the effect of small dynamic disturbances on the static maximum strength of initially imperfect shells can be studied. The manner of utilization of the analog in the present investigation is illustrated in Appendix IV.

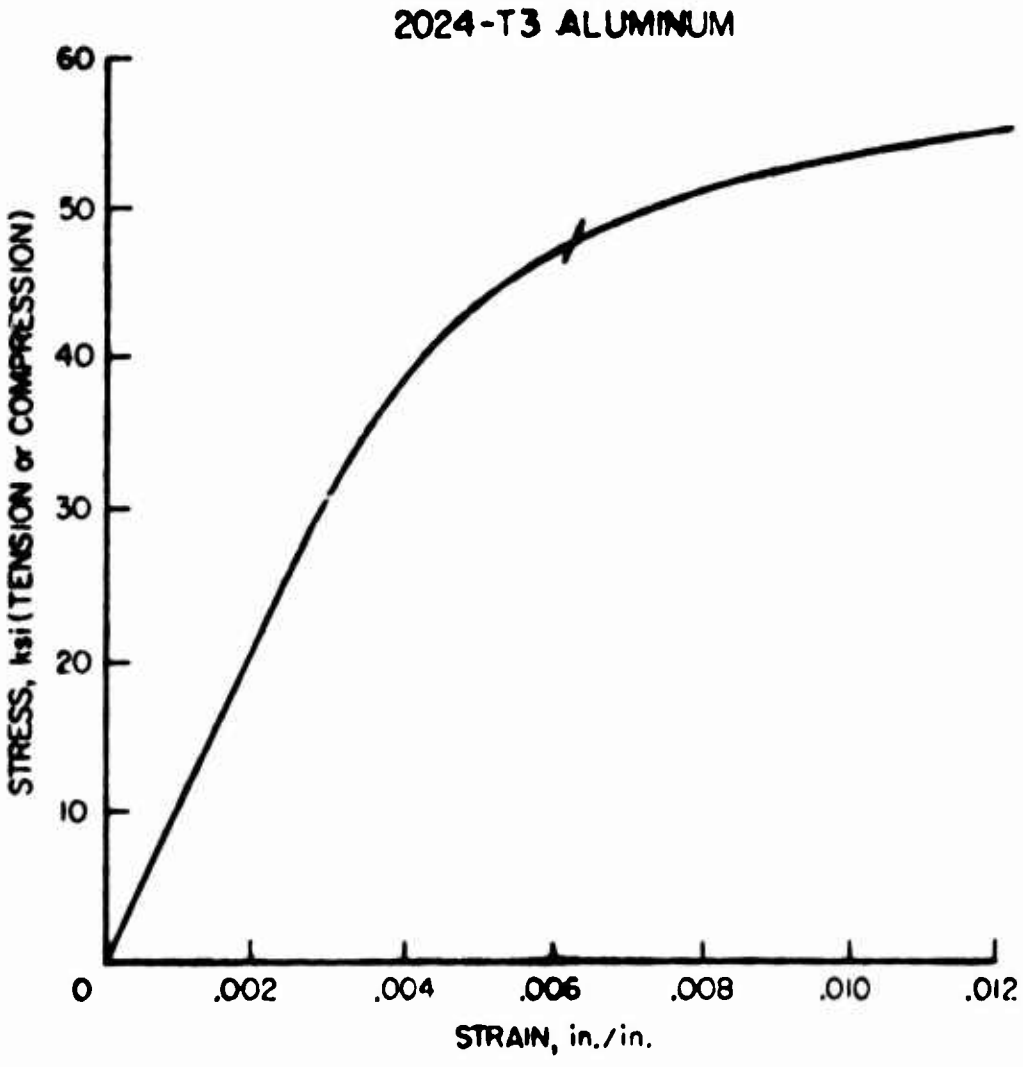

Figure 3. Stress-Strain Curve for 2024-T3 Aluminum Used in Present Inelastic Analysis.

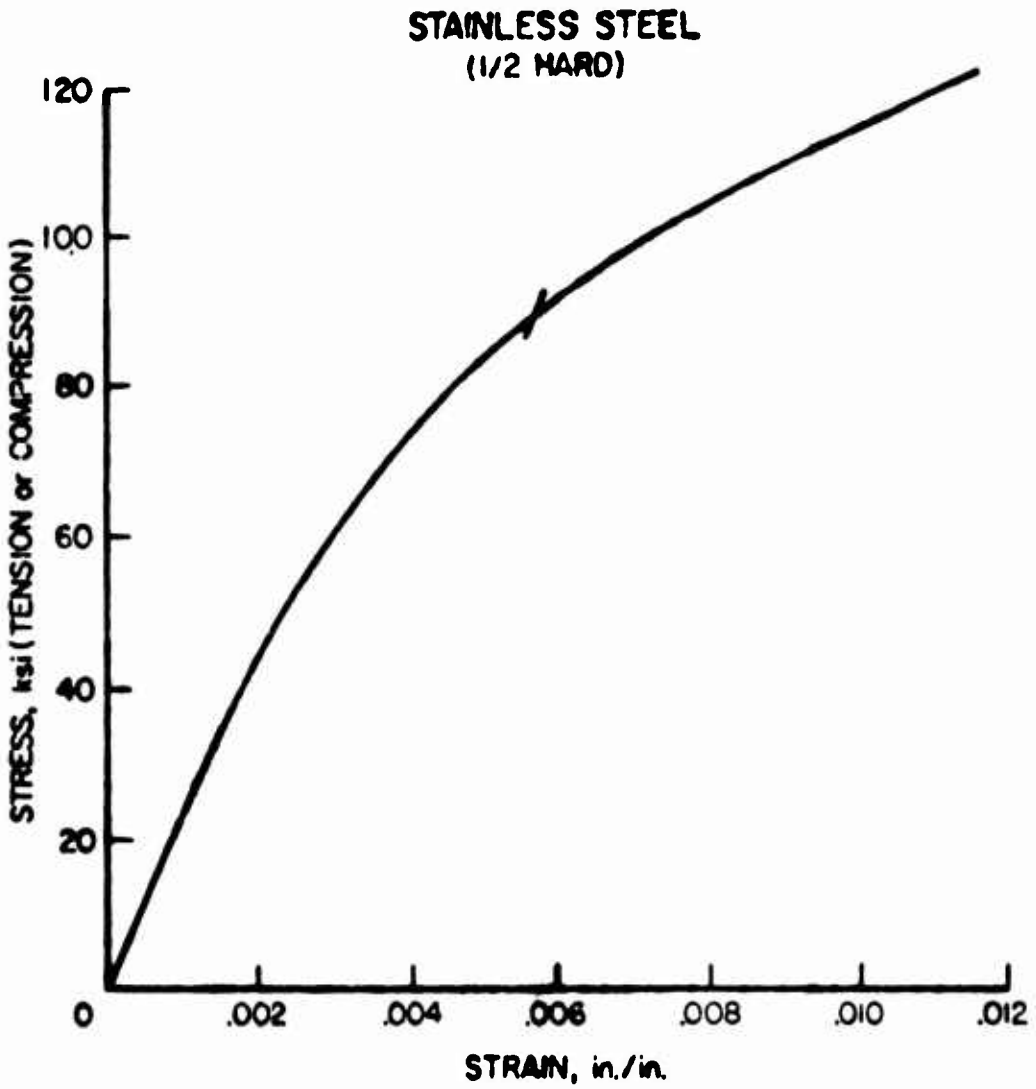

Figure 4. Stress-Strain Curve for Stainless Steel (1/2 Hard) Used in Present Inelastic Analysis.

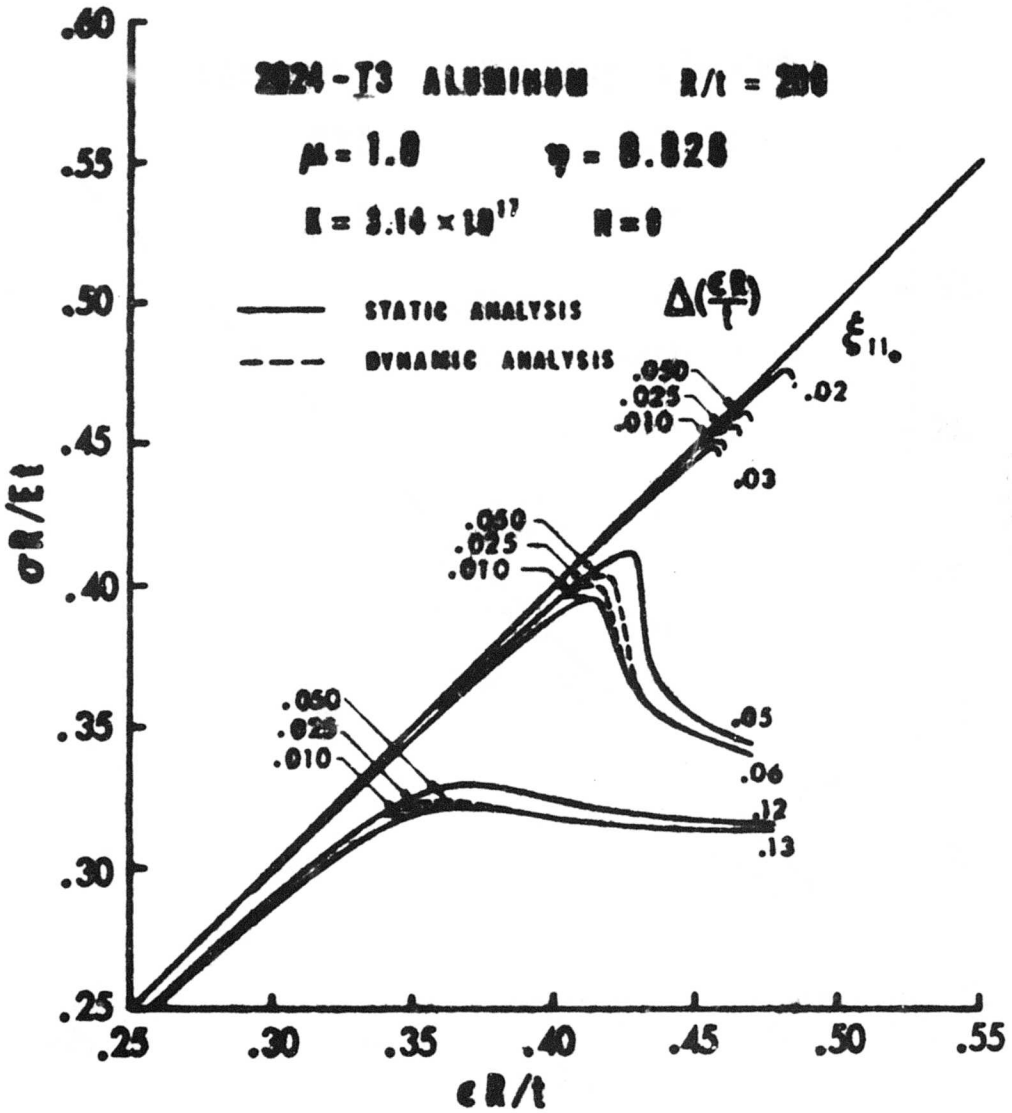

Figure 5. Family of Static and Dynamic Imperfection-Sensitive, Load-Shortening Curves for a Two-Element, 2024-T3 Aluminum Cylinder With R/t = 200.

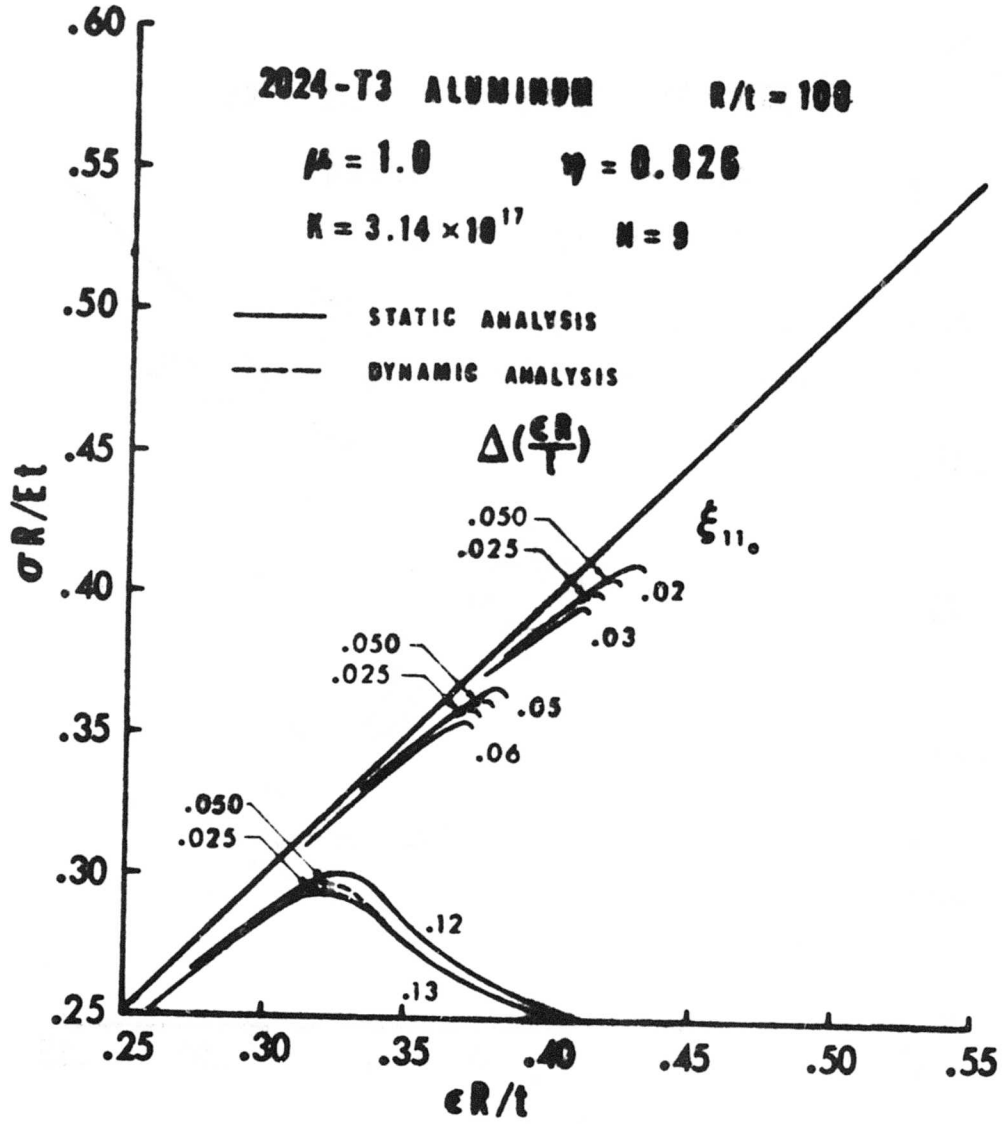

Figure 6. Family of Static and Dynamic Imperfection-Sensitive, Load-Shortening Curves for a Two-Element, 2024-T3 Aluminum Cylinder With R/t = 100.

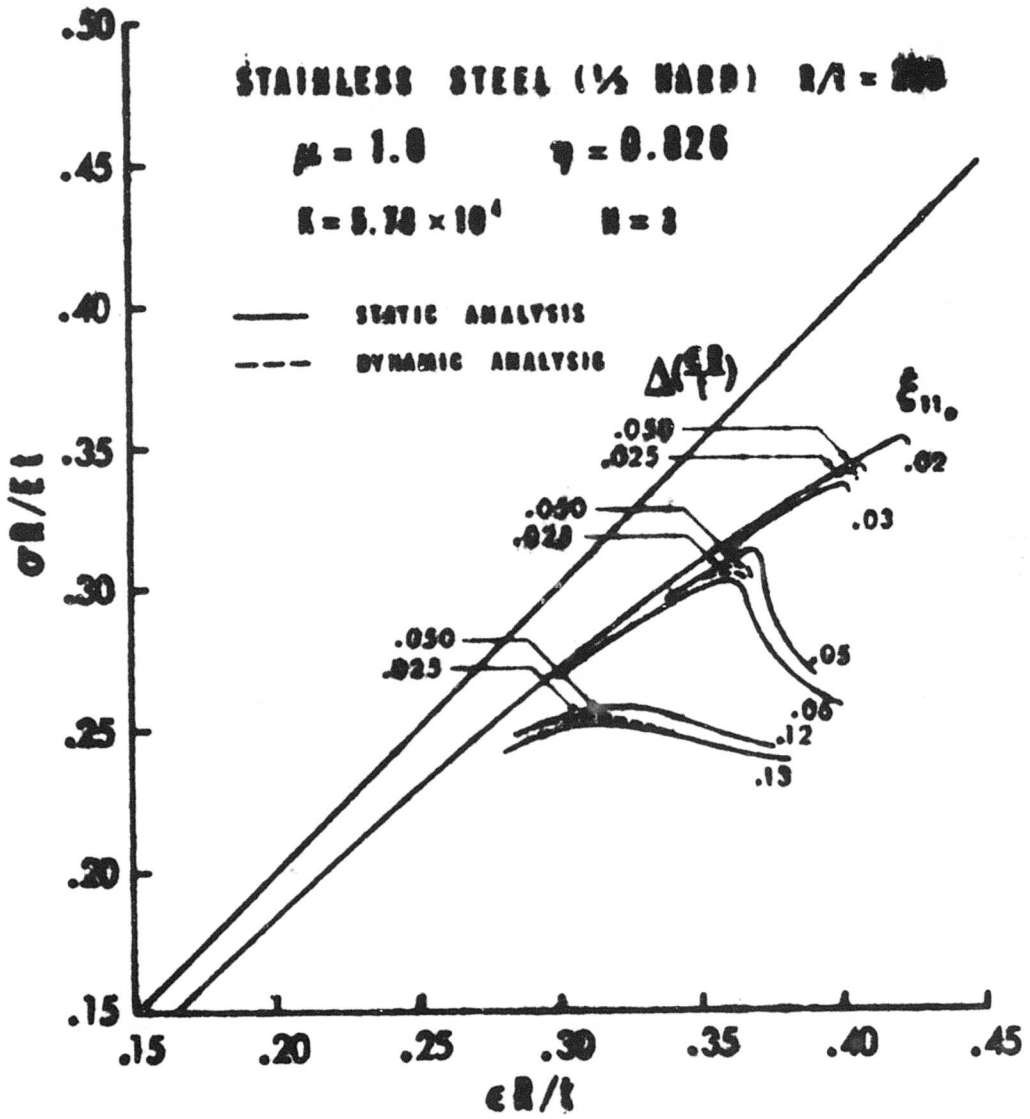

Figure 7. Family of Static and Dynamic Imperfection-Sensitive, Load-Shortening Curves for a Two-Element Stainless Steel (1/2 Hard) Cylinder With R/t = 200.

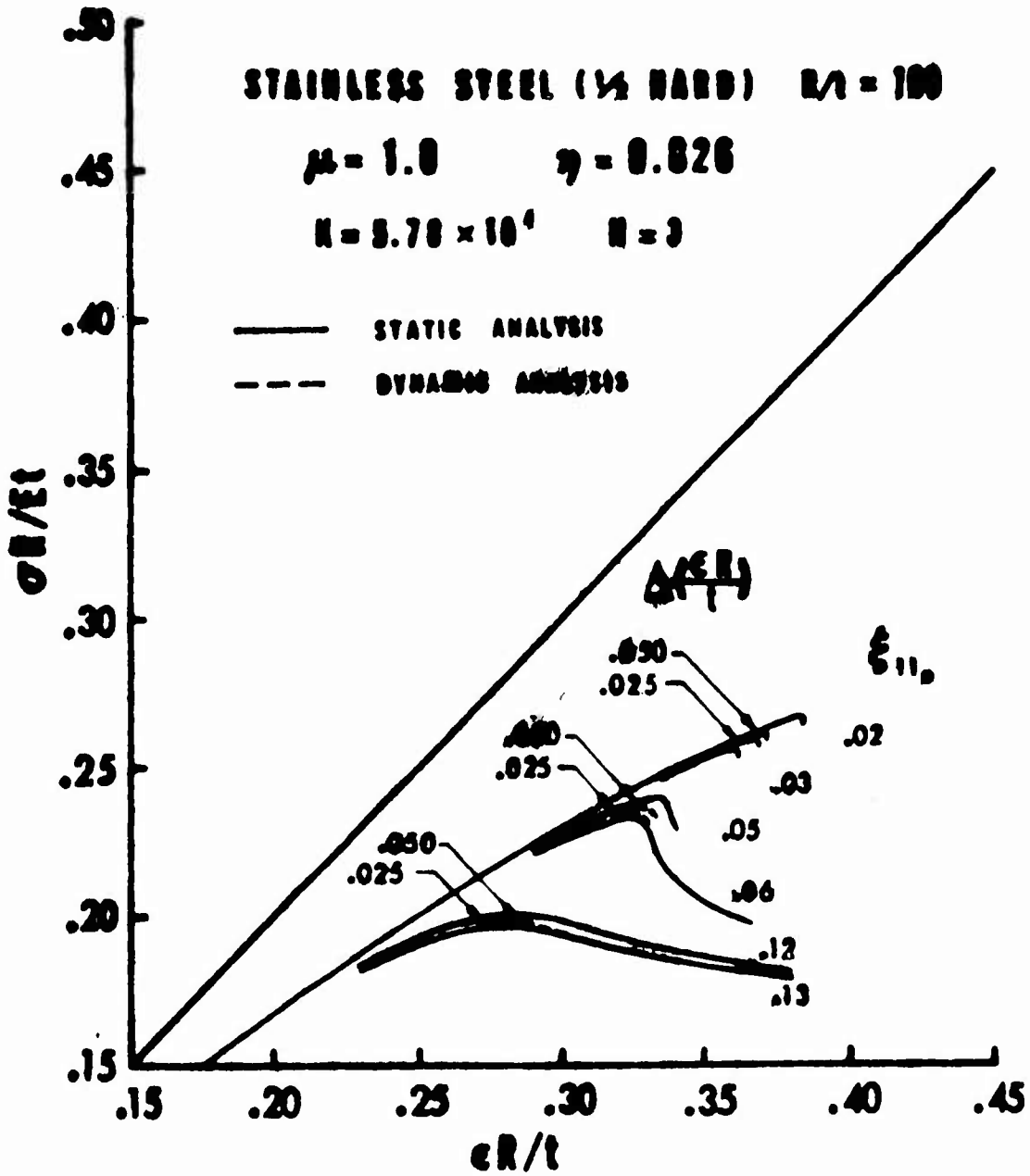

Figure 8. Family of Static and Dynamic Imperfection-Sensitive, Load-Shortening Curves for a Two-Element Stainless Steel (1/2 Hard) Cylinder With R/t = 100.

DISCUSSION AND RESULTS

The maximum strength of dynamically perturbed, initially imperfect, axially compressed, circular cylindrical shells has been studied using an analog to represent dynamic imperfection growth. A modified Hamiltonian based on the von Kármán-Donnell strain-displacement relations and a nonlinear constitutive law is incorporated to obtain Euler equations of motion of the nonlinear, though conservative, system. The effects of inertia in the equations of motion are neglected, and a dynamic imperfection component is added to the static initial imperfection to obtain a simple analog of the dynamically perturbed problem. Maximum strength, radius-to-thickness dependent, load-shortening curves are obtained for both the static problem and the analog of the dynamic problem. Two different radius-to-thickness ratios, 100 and 200, are used to demonstrate the effects on maximum strength in the elasto-plastic region. Similarly, two materials, stainless steel ($\frac{1}{2}$ hard) and 2024-T3 aluminum alloy, are used as examples of practical materials with vastly different nonlinear constitutive relations. Several different imperfection ranges are selected to correlate qualitatively the results of experimental work undertaken during the past several decades.

ELASTIC LOAD-SHORTENING RELATION

A family of imperfection-sensitive, static, linear-elastic, load-shortening curves for an isotropic, circular cylindrical shell have been produced in Figure 6 utilizing von Kármán-Donnell large-displacement theory in a modified-Reissner variational process. A Rayleigh-Ritz procedure based on a four-term trigonometric series of the same form as that of Kempner,[25] has been used in conjunction with the linearized moment-curvature relations and the middle-surface equilibrium equations to obtain the linear-elastic solution of the general problem. The results obtained represent the solution to the initially imperfect problem presented in Appendix II. The values of

the waveform parameters, $\mu = 1.0$ and $\eta = 0.826$, are selected as stationary values for the bending and buckling range based on solution results of (1) the linearized problem by Madsen and Hoff[27] and (2) the nonlinear problem by Meller and Mayers,[28] who obtained these values in the limit as the bifurcation point of linear theory is approached for a perfect shell. These values are maintained during the imperfect shell analysis in view of their collective minimum-energy property for the perfect shell.

The reduction in maximum strength with increasing initial imperfection is clearly shown in Figure 2. As small an initial deviation of 1% of the wall thickness from the perfect shape can produce a 15% reduction in initial buckling load. For an initial imperfection parameter value of about ${}^{\xi}11_{o} = 0.05$, the load-shortening curve changes from a multivalued relationship at constant eR/t, in which catastrophic snapthrough is the characteristic failure mode, to a single-valued function at constant eR/t with rapid, but continuous, reduction in load versus end shortening, and about a 30% reduction in buckling strength. The reduction in buckling strength continues until, as shown by Mayers and Meller,[28] the concept of initial maxima vanishes completely for ${}^{\xi}11_{o} \simeq 0.17$. It must be noted that the use of the four-term deflection pattern of Kempner[25] produces accurate bending, and initial buckling results; but once the initial maxima have been reached, the limitations of von Kármán-Donnell theory are surpassed and the solution fails. It was shown first by Yoshimura[29] that the very large-deflection postbuckled shape of the circular cylindrical shell is developable (no stretching of the middle surface) into a polyhedral surface consisting of identical plane triangles. In a study of the validity of von Kármán-Donnell shell theory, Mayers and Rehfield[10] showed the theory to be completely inadequate for representing very large-deflection postbuckling behavior except in the limiting case of linear elasticity and $t/R \rightarrow 0$.

In the survey papers of Hoff[1,2] and Stein,[3] thorough review is made of the possible reasons for the significant discrepancies present between theory and experiment in shell buckling under axial compression. The scatter band of test data reported through 1961 (see Reference 3) is shown in Figure 9. To obtain physically representative results in the present analysis, a range of imperfection values based on linear-elastic-analysis calculations has been selected to yield typical upper, middle, and lower bandwidth values of shell maximum strengths. A 2024-T3 aluminum alloy cylinder with $R/t = 200$ is used as a representative elastic shell, since its buckling stresses based on inelastic analysis are within 99% of the linear-elastic-analysis values.

The initial deviations from the ideal cylinder are $\xi_{11_o} = 0.02$ for the upper, 0.05 for the middle, and 0.12 for the lower regions of the bandwidth. These represent maximum strength to classical buckling strength ratios of 0.79, 0.68, and 0.55 respectively. For comparison purposes, these imperfection parameter values are retained through the inelastic analysis.

INELASTIC LOAD-SHORTENING RELATION

Addition of the nonlinear terms associated with nonzero values of the Ramberg-Osgood parameter K to the linear elastic load-shortening relation for a two-element isotropic circular cylindrical shell results in the family of radius-to-thickness, material-dependent curves (solid lines) in Figures 5 through 8. Each figure represents an imperfection-sensitive series of curves for a particular material (aluminum or stainless steel) and R/t ratio (200 or 100). The predominant failure mode remains the same, although the maxima are significantly affected relative to the aluminum cylinder of $R/t = 200$.

The major effects exemplified in the two choices of R/t and material are the transition from purely elastic to elasto-plastic behavior with R/t decrease and the significant reduction in maximum strength with

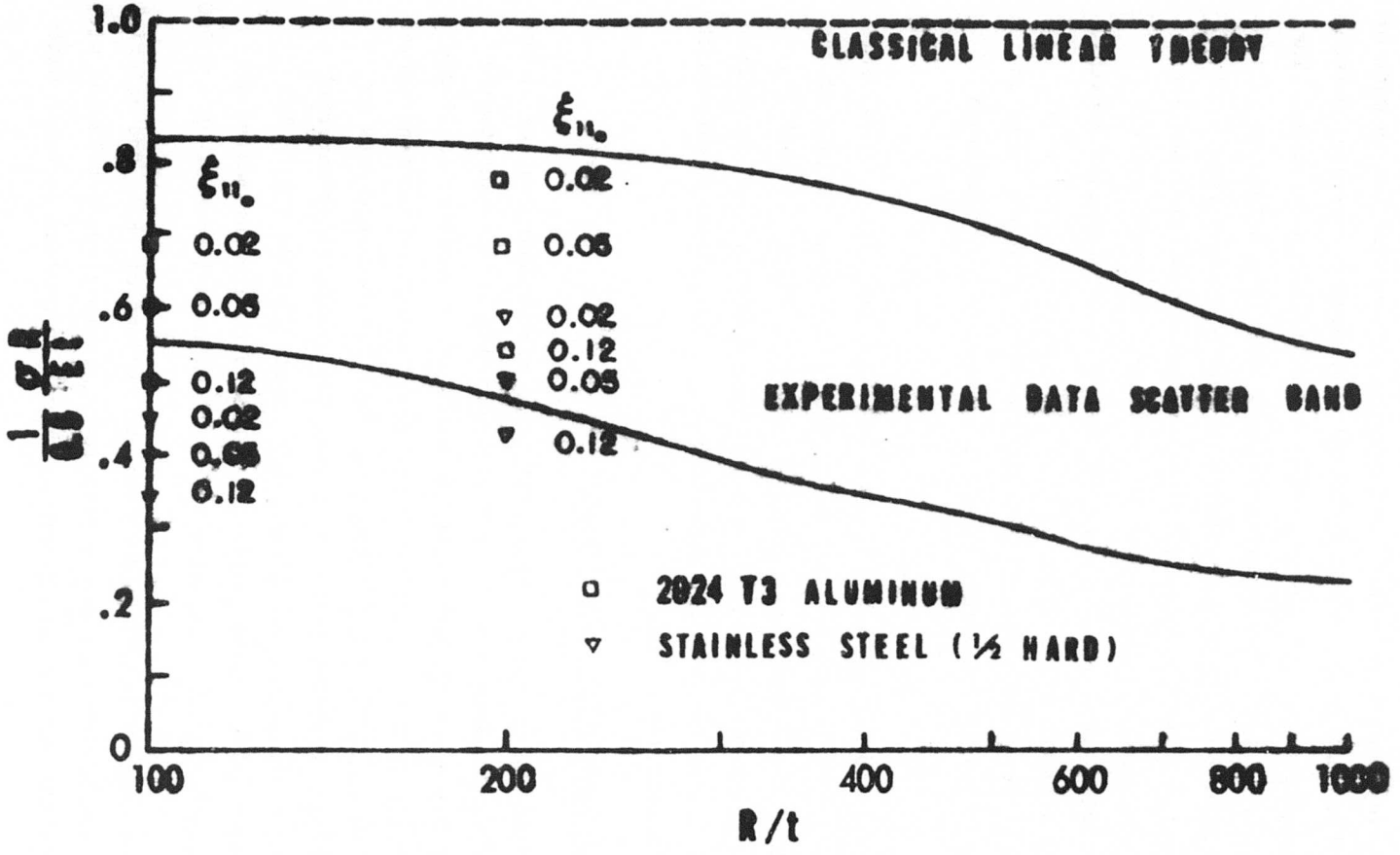

Figure 9. Experimental Buckling Loads for Axially Compressed Circular Cylindrical Shells.

decreasing values of N in the uniaxial constitutive law. In Figure 5, 2024-T3 aluminum with an R/t = 200 can be considered to act within 99% of the elastic values at all times. The R/t dependency in Figure 6 appears as a direct result of inelastic effects. The 13% reduction in maximum strength for R/t = 100 and ξ_{11_o} = 0.02 as opposed to R/t = 200 and ξ_{11_o} = 0.02 in Figure 5 results from the occurrence of local stresses exceeding the proportional limit stress of the material and the degree of material nonlinearity. In Figures 8 and 9, the same R/t -ratio effects can be observed, but with as great as a 44% reduction in maximum strength when the material is stainless steel and ξ_{11_o} remains equal to 0.02 . The highly nonlinear nature (N = 3) of the uniaxial constitutive law produces considerable softening in both the peaks and the slopes of the load-shortening curves. For these relatively low values of R/t, the peak stresses are significantly above that of the proportional limit although the lateral wall deflections are still of the order of the wall thickness. The analysis, then, is still within the kinematic limitations of von Kármán-Donnell theory discussed by Mayers and Rehfield.[10] The relatively low R/t ratios are not extreme, since practical cylinders (either stiffened or sandwich) often have "effective" radius-to-thickness ratios in the range 50 - 250 . Further, the 0.2% offset yield stress is far from exceeded.

Figure 10 is a summary curve developed from the static maximum strengths of Figures 5 through 8 by plotting them versus initial imperfection parameter ξ_{11_o} . The linear-elastic curve represents the theoretical upper bound to axial compression buckling of perfect and imperfect shells. The remaining solid curves show the reduction in maximum strength due to the combined effects of initial imperfections and material nonlinearity as a function of R/t ratio. Included, also, are imperfection "knockdown" design stresses adjusted for plastic effects as recommended in Reference 30. The range of imperfections shown in Figure 10 represents the distribution of initial imperfections that are normally used to explain the high, medium, and low maximum stresses observed in past experimental investigations (see Figure 7). At best,

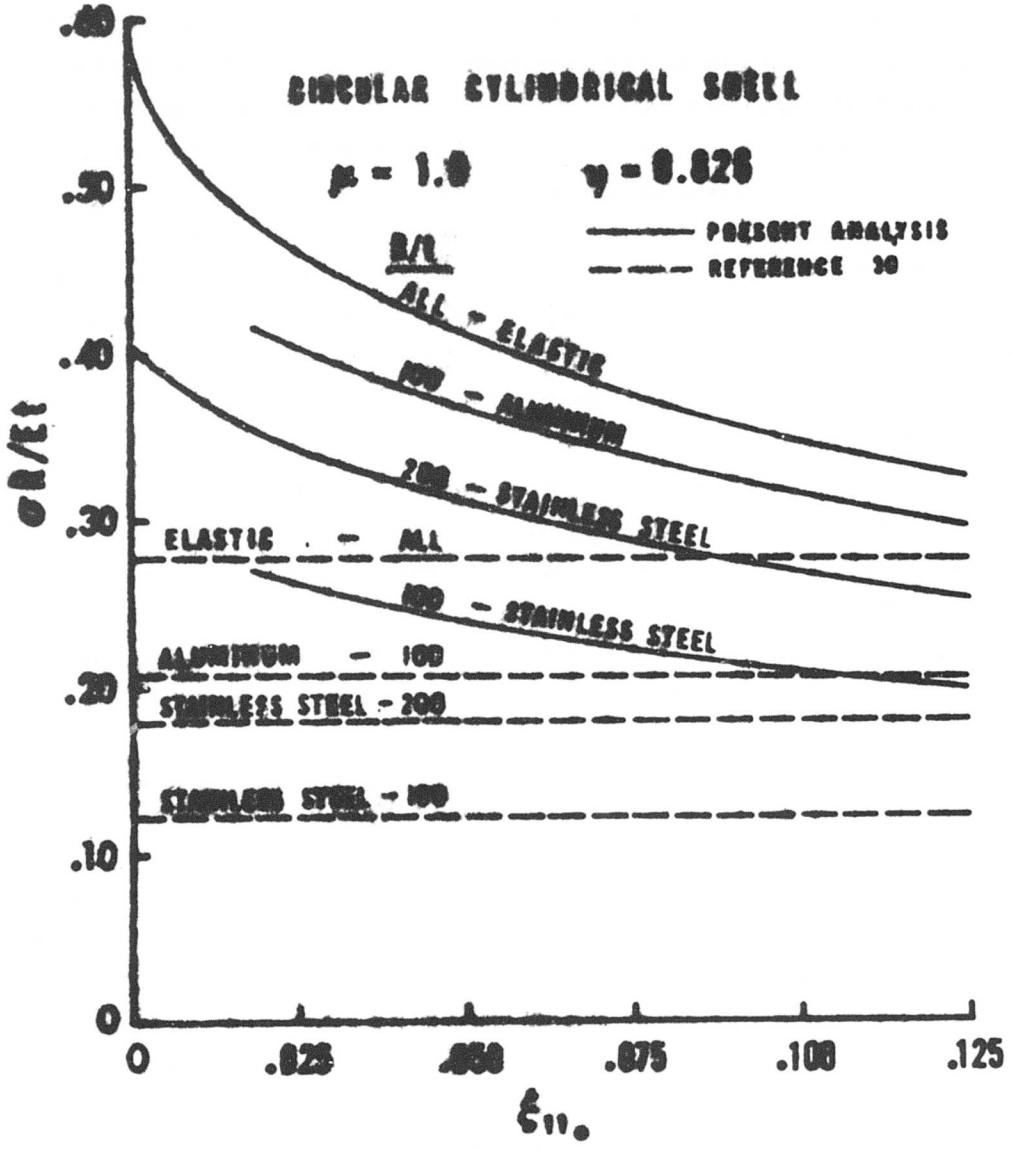

Figure 10. Prediction of Maximum Strength Versus Initial-Imperfection Parameter for 2024-T3 Aluminum and Stainless Steel (1/2 Hard) Cylinders (R/t = 100 and 200) and Comparison With a Standard Procedure.

the "knockdown" stresses of Reference 30 are still about 10% below the present results in the case of 2024-T3 aluminum and $R/t \geq 200$. For stainless steel, with an $R/t = 100$, they are about 40% below the present-analysis predictions.

These curves show that the greatest effect in maximum strength reduction may well be the initial imperfection sensitivity propounded in the literature, but that in the range of practical shell "effective" radius-to-thickness ratios, material nonlinearity can significantly affect maximum strength performance at stress levels well below those defined by the 0.2% offset yield-stress criterion. Further, the effect of material nonlinearity can contribute to the scatter of test results at a given ratio of R/t, as discussed in Reference 31.

ELASTIC DYNAMIC PERTURBATION

The effect of a dynamic perturbation on the static maximum strength of a uniformly shortened shell is assessed by incorporating the mechanism of time-dependent, initial-imperfection growth in the static analysis described in Appendix II. With inertia effects neglected, this analog is seen from Figures 5 and 6 to yield a first approximation to the actual effect of nonimpulsive dynamic disturbance of an imperfect shell under constant-rate end shortening. The growth of the initial imperfection amplitudes in sinusoidal fashion with time is related to the end-shortening rate and creates a quasi-dynamic perturbation of the static problem as described in Appendix IV. In view of the sensitivity of the elastic buckling process for thin shells to small deviations from the perfect shape, the analog approach obviously offers a much more tractable solution of the kinematically nonlinear problem and, as is discussed in the subsequent section, forms the basis for extension to the both kinematically and constitutively nonlinear problem. Since maximum loads are reached very rapidly with small increases in imperfection amplitude, it is not necessary to consider more than the first-quarter period of sinusoidal oscillation following application of the disturbance.

With the maximum amplitude of dynamic imperfection growth fixed at $\xi_{11_o} + \xi_{20} = 0.0125$, static linear elastic maximum strength load-shortening curves are constructed for $\xi_{11_o} = 0.02$, 0.05, and 0.12 as shown in Figure 5. An aluminum cylinder of $R/t = 200$ behaves in linear elastic fashion; thus, Figure 5 is valid for <u>all</u> linear-elastic cylinders of $R/t \geq 200$ within the framework of von Kármán-Donnell shell theory. Concomitantly, static load-shortening curves are also constructed for $\xi_{11_o} = 0.03$, 0.06, and 0.13, respectively. On the upper curve in each set, the sinusoidal imperfection growth is seen to commence at an eR/t value corresponding to the maximum value of $\sigma R/Et$ on the lower curve in each set. The intermediate curves represent the effect of dynamic perturbation of the initial imperfection pattern. The peaks of the intermediate curves vary as a function of the rate of application of unit end shortening and the rate of amplitude increase in the dynamic perturbation of the initial imperfection pattern. For incremental changes in eR/t of 0.05, 0.025, and 0.010, respectively, the circular frequencies of the sinusoidal oscillation are $\omega = 0.188$, 0.377, and 0.942 rad/sec, respectively. These frequencies are well out of the range of natural frequencies of even completely unloaded, simply supported, long shells of practical proportions.

From the curves of Figure 5, it is noted that more rapid application of the disturbance than that corresponding to a change in eR/t of 0.01 in about 1.7 seconds would lead to an immediate maximum in $\sigma R/Et$. For the rates shown, however, the shell either maintains its load or continues to load until a maximum is reached. The maximum load is, in general, bounded by the static analysis maximum-strength values. For relatively small imperfections, the practical case of interest, it is seen that the quasi-dynamic-analysis maximum loads are appreciably reduced from those of the static analysis and, further, that the maxima occur well prior to the amplitude of a disturbance reaching its fixed maximum of $\xi_{11_o} = 0.01$ ($\xi_{11_o} + \xi_{20_o} = 0.0125$). For such imperfection growth rates, this point is reached when an intermediate curve joins the

lower static curve in each set. For small imperfections, this region is not shown because the von Kármán-Donnell theory hypotheses have extended their validity (see Reference 10).

The results shown in Figure 5 for linear-elastic behavior would appear to indicate that imperfection-sensitive shells are further sensitive to slowly applied disturbances of the initial imperfection pattern occurring in the vicinity of the static maximum load. This phenomenon cannot be overlooked in evaluating static buckling criteria for shells. Dynamic disturbances are always present in flight environments and, to a lesser degree, in the laboratory. The rationalization of large scatter in compressed shell test data to the presence of initial imperfections (see, for example, References 1, 2, and 3) and the obviously statistical nature of static initial imperfections when viewed in the light of the results presented here suggest that dynamic disturbances of relatively low frequency occurring during the loading history cannot be ignored.

INELASTIC DYNAMIC PERTURBATION

The effect of nonimpulsive dynamic disturbance of the static loading process for linear elastic shells has been discussed in the previous section. However, of interest in the present analysis is the effect of dynamic disturbance coupled with the nonlinear elastic (or inelastic as defined herein) behavior in maximum strength analysis of compressed shells. With the use of the same unit end shortening and imperfection pattern growth rates of the linear elastic analysis (Figure 5), the inelastic analysis results are given in Figure 6 for 2024-T3 aluminum with $R/t = 100$ and in Figures 7 and 8 for stainless steel ($\frac{1}{2}$ hard) with $R/t = 200$ and 100, respectively. The uniaxial stress-strain curves used in the analyses for 2024-T3 aluminum alloy and stainless steel ($\frac{1}{2}$ hard) are shown in Figures 3 and 4, respectively. The figures show the same basic trends as those observed in the linear-elastic analysis with respect to the effects of slowly applied dynamic disturbances. As shown originally in References 14 and 15 by Mayers

and Wesenberg, the effect of material nonlinearity in materials of markedly different values of K and N is quite obvious. The material nonlinearity lowers the maximum stress parameter relative to the linear-elastic prediction, with the stainless steel cylinders being much more sensitive to stress-strain curve nonlinearity than those made of aluminum. The general softening effect of material nonlinearity tends to decrease the influence of dynamic disturbance relative to the linear-elastic results. This is understandable because of the lower $\sigma R/Et$ values involved when the maxima occur. Another point of importance is the influence of elevated-temperature environments; in general, material nonlinearity effects would be noticeable at higher radius-to-thickness ratios.

CONCLUDING REMARKS

The study of the effects of small nonimpulsive dynamic perturbations of the initial imperfection pattern of axially compressed, circular cylindrical shells has been undertaken with the use of static maximum strength theory and analysis and a suitable analog to account for initial imperfection growth during the loading process. The dependency of the analysis on nonlinear material properties is obtained with the use of stress-strain curves for 2024-T3 aluminum and stainless steel ($\frac{1}{2}$ hard). A family of load-shortening curves is developed for a representative range of static initial imperfections relative to each material and two radius-to-thickness ratios: 100 and 200. A similar set of load-shortening curves has been generated to show the effects on maximum strength of dynamic perturbations in the static initial imperfection pattern occurring during the loading process.

From the present results for both elastic and inelastic behavior in the bending and buckling of initially imperfect, axially compressed, circular cylindrical shells, consistent with the materials and geometries studied, it can be concluded that slowly applied dynamic perturbations can be still another phenomenon contributing to the reduction in classical buckling strength and the scatter in experimental data at a given value of radius-to-thickness ratio, especially in the range of "effectively" thick shells (stiffened and sandwich construction). With most investigators pursuing the perplexing behavior of compressed shells from the point of view of linear-elastic analysis, static imperfection sensitivity, and statistical techniques for identifying deleterious imperfection patterns, it is important to call attention to the real-world effects of material nonlinearity and dynamic disturbances. The latter phenomenon bears further investigation on the basis of a true dynamic analysis (inertia effects included) in view of the results presented herein developed from an analog.

LITERATURE CITED

1. Hoff, N. J., THE PERPLEXING BEHAVIOR OF THIN CIRCULAR CYLINDRICAL SHELLS IN AXIAL COMPRESSION, Israel Journal of Technology, Vol. 24, No. 1, 1966, pp. 1-28.

2. Hoff, N. J., THIN SHELLS IN AEROSPACE STRUCTURES, Astronautics and Aeronautics, Vol. 5, No. 2, February 1967, pp. 26-45.

3. Stein, M., RECENT ADVANCES IN THE INVESTIGATION OF SHELL BUCKLING, AIAA Journal, Vol. 6, No. 12, December 1968, pp. 2339-2345.

4. Donnell, L. H., and Wan, C., EFFECT OF IMPERFECTIONS ON BUCKLING OF THIN CYLINDERS AND COLUMNS UNDER AXIAL COMPRESSION, Journal of Applied Mechanics, Vol. 17, No. 1, March 1950, pp. 73-83.

5. Koiter, W. T., THE EFFECT OF AXISYMMETRIC IMPERFECTIONS ON THE BUCKLING OF CYLINDRICAL SHELLS UNDER AXIAL COMPRESSION, Lockheed Missiles and Space Company, Report 6-90-63-86, August 1963.

6. Horton, W. H., and Durham, S. C., IMPERFECTIONS, A MAIN CONTRIBUTOR TO SCATTER IN EXPERIMENTAL VALUES OF BUCKLING LOAD, International Journal of Solids and Structures, Vol. 1, 1959, p. 59.

7. Babcock, C. D., Jr., and Sechler, E. E., THE EFFECT OF INITIAL IMPERFECTIONS ON THE BUCKLING STRESS OF CYLINDRICAL SHELLS, National Aeronautics and Space Administration, NASA Technical Note D-2005, 1963.

8. Almroth, B. O., Holmes, A. M. C., and Brush, D. O., AN EXPERIMENTAL STUDY OF THE BUCKLING OF CYLINDERS UNDER AXIAL COMPRESSION, Experimental Mechanics, Vol. 4, 1963, p. 263.

9. Donnell, L. H., A NEW THEORY FOR THE BUCKLING OF THIN CYLINDERS UNDER AXIAL COMPRESSION AND BENDING, Transactions of the AMSE, Vol. 56, 1934, pp. 795-806.

10. Mayers, J., and Rehfield, L. W., FURTHER NONLINEAR CONSIDERATIONS IN THE BUCKLING OF AXIALLY COMPRESSED CIRCULAR CYLINDRICAL SHELLS, Stanford University; SUDAER 197, June 1964. Also Developments in Mechanics, Vol. 3, Part 1, New York, John Wiley and Sons, Inc., 1967, pp. 145-160.

11. Edwards, A. M., THE EFFECTS OF PLASTICITY ON THE BUCKLING AND POSTBUCKLING OF CIRCULAR CYLINDRICAL SHELLS, Thesis submitted for the degree of Doctor of Philosophy in Aeronautics and Astronautics to Stanford University, 1965.

12. Mayers, J., and Budiansky, B., ANALYSIS OF BEHAVIOR OF SIMPLY SUPPORTED FLAT PLATES COMPRESSED BEYOND BUCKLING INTO THE PLASTIC RANGE, National Advisory Committee for Aeronautics, NACA Technical Note 3368, 1955.

13. Mayers, J., and Nelson, E., ELASTIC AND MAXIMUM STRENGTH ANALYSES OF POSTBUCKLED RECTANGULAR PLATES BASED UPON MODIFIED VERSIONS OF REISSNER'S VARIATIONAL PRINCIPLE, Presented at AIAA Sixth Aerospace Sciences Meeting, AIAA Paper No. 68-171, New York, January 1968. Also Stanford University; USAAVLABS Technical Report 69-64, U.S. Army Aviation Materiel Laboratories, Fort Eustis, Virginia, July 1970, AD 872821.

14. Mayers, J., and Wesenberg, D. L., THE MAXIMUM STRENGTH OF INITIALLY IMPERFECT, AXIALLY COMPRESSED, CIRCULAR CYLINDRICAL SHELLS, Stanford University; USAAVLABS Technical Report 69-60, U.S. Army Aviation Materiel Laboratories, Fort Eustis, Virginia, August 1969, AD 862102.

15. Wesenberg, D. L., and Mayers, J., FAILURE ANALYSIS OF INITIALLY IMPERFECT, AXIALLY COMPRESSED, ORTHOTROPIC, SANDWICH AND ECCENTRICALLY STIFFENED, CIRCULAR CYLINDRICAL SHELLS, Stanford University; USAAVLABS Technical Report 69-86, U.S. Army Aviation Materiel Laboratories, Fort Eustis, Virginia, December 1969, AD 866199.

16. Rayleigh, J. W. S., THEORY OF SOUND, New York, The MacMillan Company, 2nd edition, Vol. 1, 1894, p. 403.

17. Love, A. E. H., THE MATHEMATICAL THEORY OF ELASTICITY, New York, Dover Publications, 4th edition, 1944, p. 543.

18. Flügge, W., STATIK UND DYNAMIK DER SCHALEN, Berlin, Verlag von Julius Springer, 1934, p. 115 and p. 230.

19. Reissner, E., ON TRANSVERSE VIBRATIONS OF THIN, SHALLOW ELASTIC SHELLS, Quarterly of Applied Mathematics, Vol. 13, 1955, pp. 169-176.

20. Mayers, J., and Wrenn, B. G., NONLINEAR FREE VIBRATIONS OF THIN, CIRCULAR CYLINDRICAL SHELLS, Developments in Mechanics, Vol. 4 (Proceedings of the 10th Midwestern Conference, Fort Collins, Colorado, Johnson Publishing Co., August 21-23), 1967, pp. 819-846. Also Stanford University; USAAVLABS Technical Report 69-82, U.S. Army Aviation Materiel Laboratories, Fort Eustis, Virginia, July 1970, AD 872813.

21. Hoff, N. J., DYNAMIC STABILITY OF STRUCTURES (Proceedings of an International Conference held at Northwestern University, Evanston, Illinois, October 18-20, 1965), Oxford and New York, Pergamon Press, 1966, pp. 7-41.

22. Hoff, N. J., BUCKLING AND STABILITY, The 41st Wilbur Wright Memorial Lecture, Journal of the Royal Aeronautical Society, Vol. 58, No. 3, 1954, pp. 3-52.

23. Ramberg, W., and Osgood, W. R., DESCRIPTION OF STRESS-STRAIN CURVES BY THREE PARAMETERS, National Advisory Committee for Aeronautics, NACA Technical Note 902, 1943.

24. Evenson, D. A., and Fulton, R. E., DYNAMIC STABILITY OF STRUCTURES (Proceedings of an International Conference held at Northwestern University, Evanston, Illinois, October 18-20, 1965), Oxford and New York, Pergamon Press, 1966, pp. 237-254.

25. Kempner, J., POSTBUCKLING BEHAVIOR OF AXIALLY COMPRESSED CIRCULAR CYLINDRICAL SHELLS, Journal of the Aeronautical Sciences, Vol. 21, No. 5, May 1954, pp. 329-335 and 342.

26. Tennyson, R. C., and Welles, S. W., ANALYSIS OF THE BUCKLING PROCESS OF CIRCULAR CYLINDRICAL SHELLS UNDER AXIAL COMPRESSION, University of Toronto; Institute of Aerospace Studies, UTIAS Report 129, February 1968.

27. Madsen, W. A., and Hoff, N. J., THE SNAP-THROUGH AND POSTBUCKLING EQUILIBRIUM BEHAVIOR OF CIRCULAR CYLINDRICAL SHELLS UNDER AXIAL LOAD, Stanford University; SUDAER No. 227, April 1965.

28. Meller, E., and Mayers, J., ON THE OPTIMUM PROPORTIONING OF STIFFENED CIRCULAR CURVED PLATES AND SHELLS FOR AXIAL COMPRESSION LOADING, USAAVLABS Technical Report 70-9, U.S. Army Aviation Materiel Laboratories, Fort Eustis, Virginia, March 1970, AD 871425.

29. Yoshimura, Y., ON THE MECHANISM OF BUCKLING OF A CIRCULAR CYLINDRICAL SHELL UNDER AXIAL COMPRESSION, NACA Technical Memorandum 1390, National Advisory Committee for Aeronautics, 1955.

30. Anon., BUCKLING OF THIN-WALLED CIRCULAR CYLINDERS, National Aeronautics and Space Administration SP-8007, August 1968.

31. Mayers, J., and Meller, E., MATERIAL NONLINEARITY EFFECTS IN OPTIMIZATION CONSIDERATIONS OF STIFFENED CYLINDERS AND INTERPRETATION OF TEST DATA SCATTER FOR COMPRESSIVE BUCKLING, Stanford University; USAAVLABS Technical Report 71-70, U.S. Army Air Mobility Research and Development Laboratory, Eustis Directorate, Fort Eustis, Virginia (in publication).

APPENDIX I

EQUATIONS OF MOTION AND BOUNDARY CONDITIONS DERIVED FROM MODIFIED-REISSNER FUNCTIONAL

The Reissner functional for prescribed end shortening, as contrasted with end loading, is simply

$$U'' = \iiint_V (\sigma_x \epsilon_x + \sigma_y \epsilon_y + \tau_{xy} \gamma_{xy} - F') \, dV \tag{24}$$

The von Kármán-Donnell strain-displacement relations, modified for the two-element cylinder of Figure 1 and including initial radial imperfections, are

$$\epsilon_{x_{t,b}} = \epsilon'_x \pm \epsilon''_x = u_{,x} + \frac{1}{2} w^2_{,y} + w_{o,x} w_{,x} \pm \frac{h}{2} w_{,xx}$$

$$\epsilon_{y_{t,b}} = \epsilon'_y \pm \epsilon''_y = v_{,y} + \frac{1}{2} w^2_{,y} + w_{o,y} w_{,y} - \frac{w}{R} \pm \frac{h}{2} w_{,yy}$$

$$\gamma_{xy_{t,b}} = \gamma'_{xy} \pm \gamma''_{xy} = u_{,y} + v_{,x} + w_{,x} w_{,y} + w_{o,x} w_{,y} + w_{o,y} w_{,x} \pm h w_{,xy} \tag{25}$$

The stresses in the top and bottom faces of the two-element cylinder in terms of the midsurface and bending components are

$$\sigma_{x_{t,b}} = \sigma'_x \pm \sigma''_x$$

$$\sigma_{y_{t,b}} = \sigma'_y \pm \sigma''_y$$

$$\tau_{xy_{t,b}} = \tau'_{xy} \pm \tau''_{xy} \tag{26}$$

After integration through the thickness of the two-element cross-section, the Reissner functional, Equation (24), becomes

$$U'' = t_f \int_0^L \int_0^{2\pi R} \left\{ \sigma_{x_t} \epsilon_{x_t} + \sigma_{x_b} \epsilon_{x_b} + \sigma_{y_t} \epsilon_{y_t} + \sigma_{y_b} \epsilon_{y_b} + \tau_{xy_t} \gamma_{xy_t} + \tau_{xy_b} \gamma_{xy_b} - (F_t' + F_b') \right\} dxdy \tag{27}$$

Substitution of Equations (25) and (26) into Equation (27) yields

$$U'' = t_f \int_0^L \int_0^{2\pi R} \left\{ (\sigma_{x_t} + \sigma_{x_b}) \epsilon_x' + (\sigma_{y_t} + \sigma_{y_b}) \epsilon_y' + (\tau_{xy_t} + \tau_{xy_b}) \gamma_{xy}' + (\sigma_{x_t} - \sigma_{x_b}) \epsilon_x'' + (\sigma_{y_t} - \sigma_{y_b}) \epsilon_y'' + (\tau_{xy_t} - \tau_{xy_b}) \gamma_{xy}'' - (F_t' + F_b') \right\} dxdy \tag{28}$$

The average stresses and bending moments are defined as

$$\begin{aligned} \sigma_x' &= \frac{1}{2} (\sigma_{x_t} + \sigma_{x_b}) \\ \sigma_y' &= \frac{1}{2} (\sigma_{y_t} + \sigma_{y_b}) \\ \tau_{xy}' &= \frac{1}{2} (\tau_{xy_t} + \tau_{xy_b}) \end{aligned} \tag{29}$$

and

$$\begin{aligned} M_x &= - t_f \frac{h}{2} (\sigma_{x_t} - \sigma_{x_b}) = - t_f h \sigma_x'' \\ M_y &= - t_f \frac{h}{2} (\sigma_{y_t} - \sigma_{y_b}) = - t_f h \sigma_y'' \\ M_{xy} &= t_f \frac{h}{2} (\tau_{xy_t} - \tau_{xy_b}) = t_f h \tau_{xy}'' \end{aligned} \tag{30}$$

After substitution for the average stresses and bending moments, Equations (29) and (30), and the strains, Equation (25), the Reissner functional becomes

$$U'' = 2t_f \int_0^L \int_0^{2\pi R} \left\{ \sigma_x' \left(u_{,x} + \frac{1}{2} w_{,x}^2 + w_{,x} w_{o,x} \right) + \sigma_y' \left(v_{,y} + \frac{1}{2} w_{,y}^2 + w_{,y} w_{o,y} - \frac{w}{R} \right) + \tau_{xy}' \left(u_{,y} + v_{,x} + w_{,x} w_{,y} + w_{,x} w_{o,y} + w_{o,x} w_{,y} \right) - \frac{M_x}{2t_f} w_{,xx} - \frac{M_y}{2t_f} w_{,yy} + \frac{M_{xy}}{t_f} w_{,xy} - F' \right\} dxdy \qquad (31)$$

The kinetic energy of a freely vibrating two-element circular cylindrical shell is defined as

$$T'' = \frac{1}{2} \iiint_V \rho \left\{ \left[\dot{u}^2 + \dot{v}^2 + \dot{w}^2 \right]_t + \left[\dot{u}^2 + \dot{v}^2 + \dot{w}^2 \right]_b \right\} dxdydz \qquad (32)$$

or

$$T'' = 2t_f \int_0^L \int_0^{2\pi R} \rho \left\{ \dot{u}^2 + \dot{v}^2 + \dot{w}^2 \right\} dxdy \qquad (33)$$

after integration through the thickness of the cross section.

With a Lagrangian written in terms of the Reissner functional U'' and the kinetic energy T'' as $(U'' - T'')$, the enforcement of Hamilton's principle as denoted by

$$\delta \int_{t_1}^{t_2} (U'' - T'') \, dt \qquad (34)$$

can be undertaken with simultaneous variation of the Equation (34) with respect to the free variables u, v, w, σ_x', σ_y', τ_{xy}', M_x, M_y,

and M_{xy} . Since the total differential of F' is

$$\delta F' = \frac{\partial F'}{\partial \sigma_x'} \delta\sigma_x' + \frac{\partial F'}{\partial \sigma_y'} \delta\sigma_y' + \frac{\partial F'}{\partial \tau_{xy}'} \delta\tau_{xy}' + \frac{\partial F'}{\partial M_x} \delta M_x + \frac{\partial F'}{\partial M_y} \delta M_y + \frac{\partial F'}{\partial M_{xy}} \delta M_{xy} \tag{35}$$

the resulting variation yields

$$\delta \int_{t_1}^{t_2} (U'' - T'')\, dt = 0 = 2t_f \int_{t_1}^{t_2} \int_0^L \int_0^{2\pi R}$$

$$\left\{ \delta\sigma_x' \left[u_{,x} + \frac{1}{2} w_{,x}^2 + w_{o,x} w_{,x} \right] - \delta\sigma_x' \frac{\partial F'}{\partial \sigma_x'} \right.$$

$$+ \delta\sigma_y' \left[v_{,y} + \frac{1}{2} w_{,y}^2 + w_{o,y} w_{,y} - \frac{w}{R} \right] - \delta\sigma_y' \frac{\partial F'}{\partial \sigma_y'}$$

$$+ \delta\tau_{xy}' \left[u_{,y} + v_{,x} + w_{,x} w_{,y} + w_{o,x} w_{,y} + w_{,x} w_{o,y} \right]$$

$$- \delta\tau_{xy}' \frac{\partial F'}{\partial \tau_{xy}'} - \frac{\delta M_x}{2t_f} w_{,xx} - \delta M_x \frac{\partial F'}{\partial M_x}$$

$$- \frac{\delta M_y}{2t_f} w_{,yy} - \delta M_y \frac{\partial F'}{\partial M_y} + \frac{\delta M_{xy}}{2t_f} w_{,xy} - \delta M_{xy} \frac{\partial F'}{\partial M_{xy}}$$

$$+ \sigma_x' \left[\delta u_{,x} + w_{,x} \delta w_{,x} + w_{o,x} \delta w_{,x} \right]$$

$$\left. + \sigma_y' \left[\delta v_{,y} + w_{,y} \delta w_{,y} + w_{o,y} \delta w_{,y} - \frac{\delta w}{R} \right] \right.$$

and

$$+ \tau'_{xy}\left[\delta u_{,y} + \delta v_{,x} + w_{,x}\delta w_{,y} + w_{,y}\delta w_{,x}\right.$$

$$\left. + w_{o,x}\delta w_{,y} + w_{o,y}\delta w_{,x}\right]$$

$$- \frac{M_x}{2t_f}\delta w_{,xx} - \frac{M_y}{2t_f}\delta w_{,yy} + \frac{M_{xy}}{t_f}\delta w_{,xy}$$

$$\left. - \rho\left[\dot{u}\,\delta\dot{u} + \dot{v}\,\delta\dot{v} + \dot{w}\,\delta\dot{w}\right]\right\} dxdydt \qquad (35)$$

With suitable integration by parts, Equation (36) becomes

$$2t_f \int_{t_1}^{t_2}\int_0^L\int_0^{2\pi R}\left\{\left[u_{,x} + \frac{1}{2}w_{,x}^2 + w_{o,x}w_{,x} - \frac{\partial F'}{\partial \sigma'_x}\right]\delta\sigma'_x\right.$$

$$+ \left[v_{,y} + \frac{1}{2}w_{,y}^2 + w_{o,y}w_{,y} - \frac{w}{R} - \frac{\partial F'}{\partial \sigma'_y}\right]\delta\sigma'_y$$

$$+ \left[u_{,y} + v_{,x} + w_{,x}w_{,y} + w_{o,x}w_{,y} + w_{,x}w_{o,y}\right.$$

$$\left. - \frac{\partial F'}{\partial \tau'_{xy}}\right]\delta\tau'_{xy} - \left[\frac{w_{,xx}}{2t_f} + \frac{\partial F'}{\partial M_x}\right]\delta M_x$$

$$- \left[\frac{w_{,yy}}{2t_f} + \frac{\partial F'}{\partial M_y}\right]\delta M_y + \left[\frac{w_{,xy}}{t_f} - \frac{\partial F'}{\partial M_{xy}}\right]\delta M_{xy}$$

$$- \left[\frac{\partial \sigma'_x}{\partial x} + \frac{\partial \tau'_{xy}}{\partial y} - \rho\ddot{u}\right]\delta u - \left[\frac{\partial \sigma'_y}{\partial y} + \frac{\partial \tau'_{xy}}{\partial x} - \rho\ddot{v}\right]\delta v$$

and

$$
\begin{aligned}
&- \left[\left(\sigma'_x w_{,x} + \sigma_x w_{o,x} \right)_{,x} + \left(\sigma'_y w_{,y} + \sigma'_y w_{o,y} \right)_{,y} \right. \\
&+ \left(\tau'_{xy} w_{,y} + \tau'_{xy} w_{o,y} \right)_{,x} + \left(\tau'_{xy} w_{,x} + \tau'_{xy} w_{o,x} \right)_{,y} \\
&+ \frac{1}{2t_f} \left(M_{x,xx} - 2M_{xy,xy} + M_{y,yy} \right) \\
&\left. + \frac{\sigma'_y}{R} - \rho \ddot{w} \right] \delta w \Bigg\} \, dxdydt \\
&+ 2t_f \left\{ \int_{t_1}^{t_2} \int_0^{2\pi R} \sigma'_x \delta u \Big|_0^L \, dydt \right. \\
&+ \int_{t_1}^{t_2} \int_0^L \tau'_{xy} \delta u \Big|_0^{2\pi R} \, dxdt - \rho \int_0^L \int_0^{2\pi R} \dot{u} \delta u \Big|_{t_1}^{t_2} \, dxdy \\
&+ \int_{t_1}^{t_2} \int_0^L \sigma'_y \delta v \Big|_0^{2\pi R} \, dxdt + \int_{t_1}^{t_2} \int_0^{2\pi R} \tau'_{xy} \delta v \Big|_0^L \, dydt \\
&- \rho \int_0^L \int_0^{2\pi R} \dot{v} \delta v \Big|_{t_1}^{t_2} \, dxdy \\
&+ \int_{t_1}^{t_2} \int_0^{2\pi R} \left[\sigma'_x (w_{,x} + w_{o,x}) + \tau'_{xy} (w_{,y} + w_{o,y}) \right. \\
&\left. \left. + \frac{1}{2t_f} \left(M_{x,x} - 2M_{xy,y} \right) \right] \delta w \Big|_0^L \, dydt
\end{aligned}
$$

and

$$+ \int_{t_1}^{t_2} \int_{0}^{L} \left[\sigma'_y (w_{,y} + w_{o,y}) + \tau'_{xy} (w_{,x} + w_{o,x}) \right.$$

$$\left. + \frac{1}{2t_f} \left(M_{y,y} - 2M_{xy,x} \right) \right] \delta w \Big|_{0}^{2\pi R} \, dxdt$$

$$- \int_{t_1}^{t_2} \int_{0}^{2\pi R} \frac{M_x}{2t_f} \delta w_{,x} \Big|_{0}^{L} \, dydt$$

$$+ \int_{t_1}^{t_2} \int_{0}^{L} \frac{M_{xy}}{t_f} \delta w_{,x} \Big|_{0}^{2\pi R} \, dxdt$$

$$- \int_{t_1}^{t_2} \int_{0}^{L} \frac{M_y}{2t_f} \delta w_{,y} \Big|_{0}^{2\pi R} \, dxdt$$

$$- \rho \int_{0}^{L} \int_{0}^{2\pi R} \dot{w} \delta w \Big|_{t_1}^{t_2} \, dxdy = 0 \qquad (37)$$

For Equation (37) to vanish simultaneously for arbitrary variations in the states of generalized stress and displacement, each of the terms must vanish independently. The resulting equations of motion and constitutive relations are as follows:

Equations of motion:

$$\sigma'_{x,x} + \tau'_{xy,y} = \rho \ddot{u} \qquad (38)$$

$$\tau'_{xy,x} + \sigma'_{y,y} = \rho \ddot{v} \qquad (39)$$

and

$$\left[\sigma_x'(w_{,x} + w_{o,x})\right]_{,x} + \left[\sigma_y'(w_{,y} + w_{o,y})\right]_{,y}$$

$$+ \left[\tau_{xy}'(w_{,y} + w_{o,y})\right]_{,x} + \left[\tau_{xy}'(w_{,x} + w_{o,x})\right]_{,y}$$

$$+ \frac{1}{2t_f}\left(M_{x,xx} - 2M_{xy,xy} + M_{y,yy}\right) + \frac{\sigma_y'}{R} = \rho\ddot{w} \qquad (40)$$

Substitution of Equations (38) and (39) into Equation (40) simplifies the lateral equilibrium equation to the form

$$\sigma_x'(w_{,xx} + w_{o,xx}) + \sigma_y'(w_{,yy} + w_{o,yy}) + 2\tau_{xy}'(w_{,xy} + w_{o,xy})$$

$$+ \frac{1}{2t_f}\left(M_{x,xx} - 2M_{xy,xy} + M_{y,yy}\right) + \frac{\sigma_y'}{R}$$

$$= \rho\left[\ddot{w} - \ddot{u}(w_{,x} + w_{o,x}) - \ddot{v}(w_{,y} + w_{o,y})\right] \qquad (41)$$

Stress-displacement relations:

$$\frac{\partial F'}{\partial \sigma_x'} = u_{,x} + \frac{1}{2}w_{,x}^2 + w_{o,x}w_{,x} \qquad (42)$$

$$\frac{\partial F'}{\partial \sigma_y'} = v_{,y} + \frac{1}{2}w_{,y}^2 + w_{o,y}w_{,y} - \frac{w}{R} \qquad (43)$$

$$\frac{\partial F'}{\partial \tau_{xy}} = u_{,y} + v_{,x} + w_{,x}w_{,y} + w_{o,x}w_{,y} + w_{,x}w_{o,y} \qquad (44)$$

Moment-curvature relations:

$$\frac{\partial F'}{\partial M_x} = -\frac{1}{2t_f} w_{,xx} \tag{45}$$

$$\frac{\partial F'}{\partial M_y} = -\frac{1}{2t_f} w_{,yy} \tag{46}$$

$$\frac{\partial F'}{\partial M_{xy}} = \frac{1}{t_f} w_{,xy} \tag{47}$$

The boundary condition combinations involving generalized stress and displacement at the ends of the shell, $x = 0$ and $x = L$, are

$$\int_{t_1}^{t_2} \int_{0}^{2\pi R} \sigma_x' \delta u \Big|_0^L \, dy dt = 0 \tag{48}$$

$$\int_{t_1}^{t_2} \int_{0}^{2\pi R} \tau_{xy}' \delta v \Big|_0^L \, dy dt = 0 \tag{49}$$

$$\int_{t_1}^{t_2} \int_{0}^{2\pi R} M_x \delta w_{,x} \Big|_0^L \, dy dt = 0 \tag{50}$$

$$\int_{t_1}^{t_2} \int_{0}^{2\pi R} \left[\sigma_x'(w_{,x} + w_{o,xx}) + \tau_{xy}'(w_{,y} + w_{o,y}) + \frac{1}{2t_f}\left(M_{x,x} - 2M_{xy,y}\right)\right] \delta w \Big|_0^L \, dy dt = 0 \tag{51}$$

With inertia effects neglected, enforcement of Hooke's law, and $2t_f \rightarrow t$ (the thickness of a homogeneous, isotropic shell), the set of equations and boundary conditions given by Equations (38), (39), and (41) through (51) reduces to the von Kármán-Donnell shell theory. With enforcement of Hooke's law, $2t_f \rightarrow t$, and the inertia terms due to motion in the axial and circumferential directions neglected in Equation (41) in accordance with the conclusion of Reissner,[19] the set of equations is that governing the nonlinear free vibrations of shallow shells given in, for example, Reference 20.

APPENDIX II

METHOD OF SOLUTION FOR TWO-ELEMENT, LINEAR-ELASTIC CIRCULAR CYLINDER

Substitution of the assumed radial and midsurface displacement functions (Equations (18) and (19)), the assumed midsurface and bending stress distributions (Equations (20) and (21)), and the prescribed initial imperfection pattern (Equation (22)) into the modified Hamiltonian represented by Equation (16), followed by integration over the volume of the cylinder material, yields

$$\bar{H}'' = \int_{t_1}^{t_2} \frac{(U'' - T'')}{2Et_f(2\pi RL/4)}\,dt = \int_{t_1}^{t_2} \left\{ 4\frac{\sigma}{E} - \frac{\sigma}{E}\mu^2\eta\frac{h}{R}\left[\frac{1}{2}\xi_{11}^2 + 4\xi_{20}^2 \right.\right.$$

$$+ \left.\xi_{11}\xi_{11_o} + 8\xi_{20}\xi_{20_o}\right] - 2A_{11}\mu^2\eta\frac{h}{R}\left[(\xi_{11} + \xi_{11_o})(\xi_{20} + \xi_{02})\right.$$

$$+ \left.\xi_{20_o}\xi_{11} - \frac{1}{2\eta}\xi_{11}\right] - 16A_{22}\mu^2\eta\frac{h}{R}\left[\xi_{02}(\xi_{20} + \xi_{20_o})\right]$$

$$- 2A_{31}\mu^2\eta\frac{h}{R}\left[\xi_{11}\xi_{20} + \xi_{11_o}\xi_{20} + \xi_{20_o}\xi_{11}\right] - 2A_{13}\mu^2\eta\frac{h}{R}\left[\xi_{02}(\xi_{11} + \xi_{11_o})\right]$$

$$- A_{20}\mu^2\eta\frac{h}{R}\left[\xi_{11}^2 + 2\xi_{11}\xi_{11_o} - \frac{8}{\eta}\xi_{20}\right] - A_{02}\mu^2\eta\frac{h}{R}\left[\xi_{11}^2 + 2\xi_{11}\xi_{11_o}\right]$$

$$- \left(\frac{\sigma}{E}\right)^2 - \frac{1}{2}\left[(A_{11}^2 + 16A_{22}^2)(1 + \mu^2)^2 + A_{13}^2(9 + \mu^2)^2\right.$$

$$+ \left.A_{31}^2(1 + 9\mu^2)^2 + 32(A_{02}^2 + \mu^4 A_{20}^2)\right]$$

and

$$
\begin{aligned}
&- \mu^2 \eta \frac{h}{R} \left[\frac{1}{2} a_{11} \xi_{11} + 4 a_{20} \xi_{20} + \frac{1}{2} b_{11} \xi_{11} + 4 b_{02} \xi_{02} - d_{11} \xi_{11} \right] \\
&- \frac{1}{2} \left[a_{11}^2 + 2 a_{20}^2 + 2 a_{02}^2 + \mu^4 (b_{11}^2 + 2 b_{20}^2 + 2 b_{02}^2) \right. \\
&\left. - 2 \nu \mu^2 (a_{11} b_{11} + 2 a_{20} b_{20} + 2 a_{02} b_{02}) + 2(1+\nu) \mu^2 d_{11}^2 \right] \\
&- (\bar{U}'')_{\text{inelastic}} \\
&\left. - \frac{1}{2} \frac{\rho}{E} \left[\frac{4}{3} \dot{e}^2 L^2 + h^2 (\dot{\xi}_{11}^2 + 2 \dot{\xi}_{20}^2 + 2 \dot{\xi}_{02}^2) \right] \right\} dt
\end{aligned}
\tag{52}
$$

where $(\bar{U}'')_{\text{inelastic}}$ is the contribution of nonlinear material behavior in the Reissner formulation. It is given by

$$
(\bar{U}'')_{\text{inelastic}} = \frac{1}{2} \int_0^L \int_0^{2\pi R} \frac{K}{(N+1)} \left[\left(\frac{\sigma_{\text{eff}}}{E} \right)_t^{N+1} + \left(\frac{\sigma_{\text{eff}}}{E} \right)_b^{N+1} \right] \frac{dxdy}{(2\pi RL/4)} \tag{53}
$$

where σ_{eff} is defined in terms of the membrane and bending stresses through Equations (10) and (26).

For the elastic case, $K = 0$ and, therefore, $(U'')_{\text{inelastic}}$ vanishes. In the resulting set of equations, the 13 generalized stress coefficients can easily be expressed explicitly in terms of the free average stress and displacement parameters through enforcement of Hooke's law. The system, as a result, is reducible to only four equations in terms of the four independent variables ξ_{11}, ξ_{20}, ξ_{02}, and $\sigma R/Et$ and may be solved numerically for prescribed values of e as well as ξ_{11_o}, ξ_{20_o}, μ, and η, the initial waveform parameters; a relationship between $(\sigma R/Et)$ and (eR/t) can then be constructed in the form of a

load-shortening curve. Although ξ_{20_o} is an initial waveform parameter, in view of the justifications reported in References 20, 26, and 29, ξ_{20} is taken equal to $\xi_{11_o}/4$ throughout the present analysis.

With the inertia effects included, all arbitrary coefficients of the assumed displacement and stress distributions become functions of time. Thus, the variational process in such a case leads to a set of time-dependent ordinary differential equations. These equations together with given initial and loading conditions define a particular problem. For relatively slow end shortening, the static maximum strength solution is assumed to be little affected by the dynamics of the buckling process for the initially imperfect shell. As a result, this type of problem is not of interest herein as is, of course, the impulsive loading problem. Of concern is the effect of a dynamic perturbation of the initial imperfection pattern as the shell is shortened into the vicinity of the end-shortening magnitude corresponding to maximum load. The effect could be represented by retaining inertia effects in the problem formulation, adding a periodic component to the existing applied constant-rate unit end shortening $e = \dot{e}t$, and specifying the time and initial conditions relative to the appearance of the disturbance. In view of the complexity of the static maximum-strength analysis and the sensitivity of the load-shortening curve to initial imperfections and nonlinear material behavior, it appears reasonable to consider the presence of a small dynamic disturbance by neglecting inertia effects and introducing an analog to estimate the first-order influence of such a disturbance on maximum load. The analog is described in Appendix IV.

When the inertia effects are neglected and the analog is not in use, the problem solution yields identically the results obtained previously by Mayers et al.[14,28] for imperfect, inelastic (two-element model) and elastic (conventional model) unstiffened shells, respectively. When the stress-strain law is linear and imperfections are absent (perfect shell), the results of References 14 and 28 are identical and equivalent to those first obtained by Kempner.[25]

APPENDIX III

REISSNER FUNCTIONAL FOR THE CIRCULAR CYLINDRICAL SHELL – THE EQUIVALENT STATIC PROBLEM

With time dependence and inelastic effects neglected (K = 0) in Equation (52) of Appendix II, the Reissner functional reduces to

$$\left(\frac{U''}{VE}\right)_{\text{elastic}} = 4\frac{\sigma}{E} - \frac{\sigma}{E}\mu^2\eta\frac{h}{R}\left[\frac{1}{2}\xi_{11}(\xi_{11} + 2\xi_{11_o}) + 4\xi_{20}(\xi_{20} + 2\xi_{20_o})\right]$$

$$- 2A_{11}\mu^2\eta\frac{h}{R}\left[(\xi_{11} + \xi_{11_o})(\xi_{20} + \xi_{20_o}) + \xi_{20_o}\xi_{11} - \frac{1}{2\eta}\xi_{11}\right]$$

$$- 16A_{22}\mu^2\eta\frac{h}{R}\left[\xi_{02}(\xi_{20} + \xi_{20_o})\right]$$

$$- 2A_{31}\mu^2\eta\frac{h}{R}\left[\xi_{11}\xi_{20} + \xi_{11_o}\xi_{20} + \xi_{20_o}\xi_{11}\right]$$

$$- 2A_{13}\mu^2\eta\frac{h}{R}\left[\xi_{02}(\xi_{11} + \xi_{11_o})\right]$$

$$- A_{20}\mu^2\eta\frac{h}{R}\left[\xi_{11}^2 + 2\xi_{11}\xi_{11_o} - \frac{8}{\eta}\xi_{20}\right]$$

$$- A_{02}\mu^2\eta\frac{h}{R}\left[\xi_{11}^2 + 2\xi_{11}\xi_{11_o}\right]$$

$$- \left(\frac{\sigma}{E}\right)^2 - \frac{1}{2}\left[(A_{11}^2 + 16A_{22}^2)(1 + \mu^2)^2 + A_{13}^2(9 + \mu^2)^2\right.$$

$$\left. + A_{31}^2(1 + 9\mu^2)^2 + 32(A_{02}^2 + \mu^4 A_{20}^2)\right]$$

and

$$- \mu^2 \eta \frac{h}{R} \left[\frac{1}{2} a_{11} \xi_{11} + 4 a_{20} \xi_{20} + \frac{1}{2} b_{11} \xi_{11} + 4 b_{02} \xi_{02} - d_{11} \xi_{11} \right]$$

$$- \frac{1}{2} \left[a_{11}^2 + 2 a_{20}^2 + 2 a_{02}^2 + \mu^4 (b_{11}^2 + 2 b_{20}^2 + 2 b_{02}^2) \right.$$

$$\left. - 2 \nu \mu^2 (a_{11} b_{11} + 2 a_{20} b_{20} + 2 a_{02} b_{02}) + 2(1 + \nu) \mu^2 d_{11}^2 \right] \quad (54)$$

This functional is identical to that developed originally in Reference 14 .

APPENDIX IV

DYNAMIC ANALOG CONSIDERATIONS

The use of an analog to assess the effects of dynamic perturbations on the maximum strength of initially imperfect, uniformly shortened, circular cylindrical shells is demonstrated in this appendix. The analog makes use of the concept of time-dependent, initial-imperfection growth occurring in the buckling-sensitive region of a compressed shell to represent the addition of a small, nonimpulsive dynamic disturbance to an essentially static loading situation for a flight vehicle structural shell. The effects of small disturbances on maximum strength predictions for specific aluminum and stainless steel cylinders are shown in Figures 5 through 8 and summarized in Figure 10.

As noted from Equation (22), the additional, time-dependent initial imperfection is

$$\Delta w_o(t) = \left(\xi_{11_o} \cos \frac{\pi x}{\lambda_x} \cos \frac{\pi y}{\lambda_y} + \xi_{20} \cos \frac{2\pi x}{\lambda_x} \right) \sin \omega t \qquad (55)$$

This perturbation in the conventional (static) maximum strength analysis provides a reasonable first approximation to the occurrence of inertia effects and a qualitative appraisal of the reduction in shell maximum strength to be expected either in the laboratory or flight environment where, at least, small inertial loads can easily occur in a statically loaded, imperfect shell structure loaded in the vicinity approaching the static stability point.

With reference to an end-shortening controlled laboratory test machine, the unit-shortening rate $\dot{e}$ is assumed to be 3×10^{-5} in./in./sec. Such a rate would cause classical buckling of a perfect shell of $R/t = 200$ to occur in about 100 seconds; the rate is sufficiently slow as to preclude any considerations of buckling under relatively short-duration loading.

For initially imperfect shells, defined by given values of $\xi 11_o$ (it is assumed that $\xi 20_o = \xi 11_o/4$ (see Appendix II)), static load-shortening curves are developed for three pairs of cases: $\xi 11_o = 0.02$ and 0.03, $\xi 11_o = 0.05$ and 0.06, and $\xi 11_o = 0.12$ and 0.13. As indicated in "DISCUSSION AND RESULTS", the first value of $\xi 11_o$ in each pairing has been selected to correlate maximum strength predictions with the bandwidth of experimental data at $R/t = 200$ (see Figure 9). The latter value of $\xi 11_o$ in each pairing is simply a static reference bound with which the effects of varying rate, time-dependent initial imperfection growths can be compared. The onset of initial imperfection growth is assumed to occur at a value of end shortening parameter eR/t which gives the stress level on the first $\xi 11_o$ curve corresponding to the maximum stress level on the second $\xi 11_o$ curve in a set of pairings. For each of the three sets, three circular frequencies of oscillation are selected consistent with the unit shortening rate of 3×10^{-5} in./in./sec. These are illustrated in Figure 11(a), where the end shortening parameter eR/t is plotted versus the nondimensional time parameter ωt. The growth of the total initial imperfection parameter $(\xi 11_o + \xi 20_o)$ to a value of 0.0125 in a quarter-period of the sinusoidal oscillation is shown in Figure 11(b), also as a function of ωt. Only a quarter-period need be considered, since the maximum load of the dynamically perturbed shell occurs within this range. A cross plot of imperfection growth to maximum amplitude $(\xi 11_o + \xi 20_o)$ as a function of end-shortening parameter eR/t obtained from Figure 4 is presented in Figure 12.

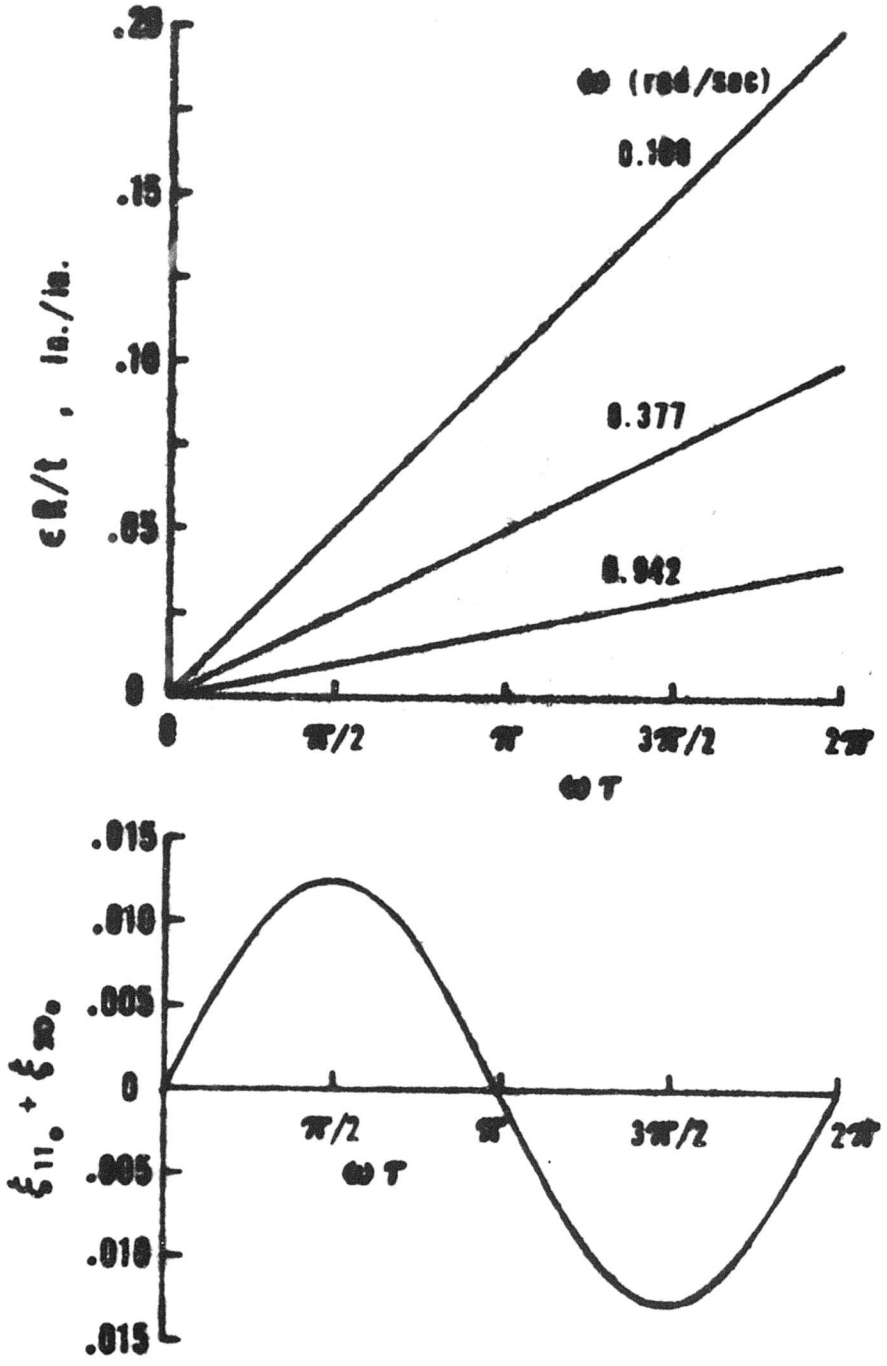

Figure 11. Variations of Dynamic Imperfection Amplitude Growth and Unit End Shortening With Time.

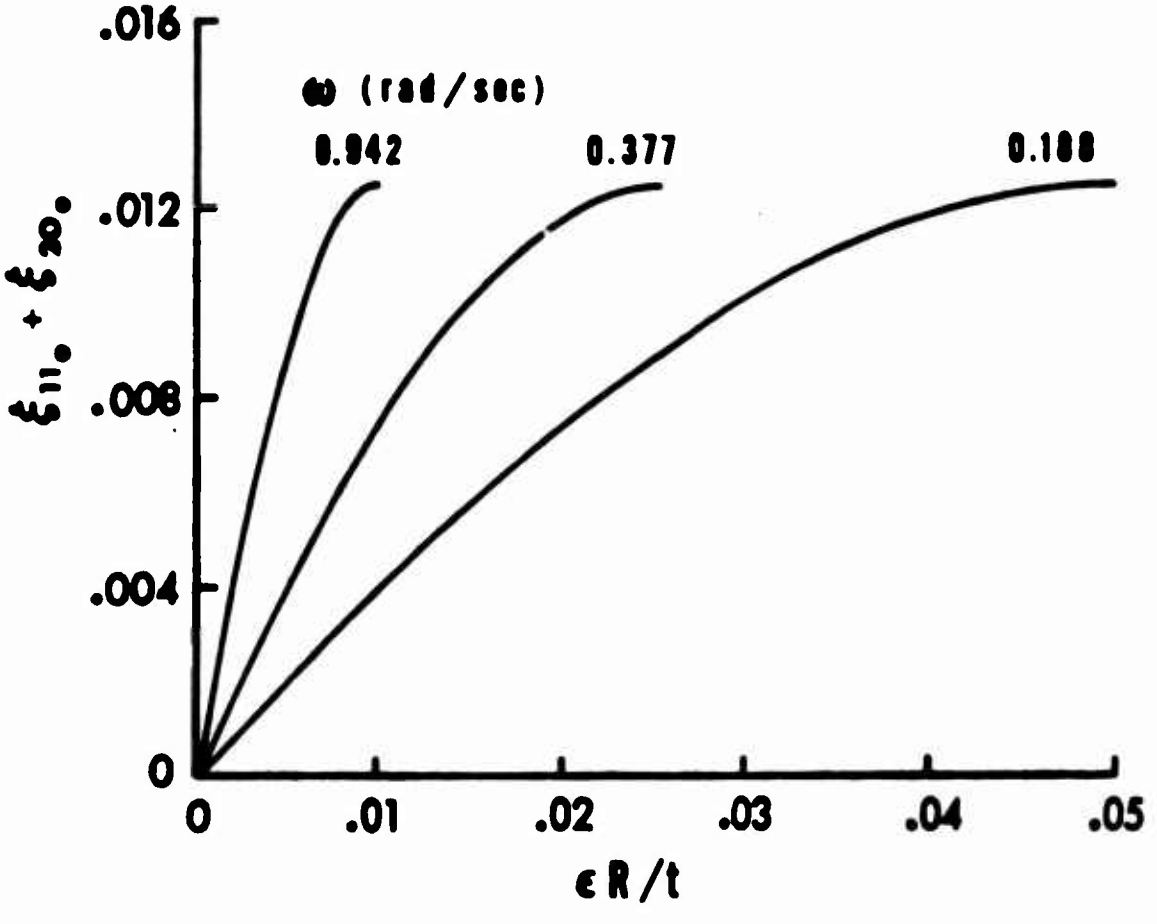

Figure 12. Variation of Dynamic Imperfection Amplitude Growth and Unit End Shortening.